An Appraisal of Tiros III Radiation Data for Southeast Asia

by
U. Radok

Colorado
State
University

Department of
Atmospheric Science

Paper No. 102

AN APPRAISAL OF TIROS III RADIATION DATA

FOR SOUTHEAST ASIA

by

U. Radok

Colorado State University

Department of Atmospheric Science
Colorado State University
Fort Collins, Colorado

August 1966

Atmospheric Science Paper No. 102

AN APPRAISAL OF TIROS III RADIATION DATA

FOR SOUTHEAST ASIA

by

U. Radok*

Department of Atmospheric Science
Colorado State University
Fort Collins, Colorado

Abstract

A short period of TIROS III radiation observations and con-
current synoptic data for Southeast Asia have been examined, as
an experiment in the use of satellite radiation data. The areas of
low radiation, usually given exclusive attention in such work, are
found to be in reasonable agreement with dynamic and general
meteorological expectations. A slight association is established
between low radiation intensity and the occurrence of heavy rain,
especially for occasions when the satellite passed <u>after</u> the rainfall
had been most intense.

For the regions of intermediate radiation intensity, constituting
the largest part of all radiation fields, it is suggested that the
"texture" of the smoothed radiation surface (measured by the local
change in radiation intensity with nadir angle and possibly with
azimuth angle as well) is determined primarily by the geometry of
the cloud fields viewed. A simple calculation suggests that this
effect is much more significant than limb darkening, and that its
consideration may add significantly to the value of satellite radiation
measurements as a meteorological tool, especially in tropical
regions.

*On leave from the Meteorology Department, University of Melbourne,
Australia.

1. Introduction

The addition of infrared radiation records to cloud photos taken in the visible part of the spectrum has greatly enlarged the potential scope of satellites as meteorological tools. Especially the combination of information for two or more of the four radiation channels operated by the present radiation satellites promises to make possible very sophisticated deductions about the state of the atmosphere (cf. e.g. Möller 1962) although certain difficulties have emerged in attempts to put these ideas into practice (Bandeen, Kunde, Nordberg, and Thompson, 1964). But even a single channel like that covering the atmospheric window (8-12, channel 2) offers for the first time the chance of confirming and testing ideas about the earth's radiation budget which so far have rested largely on indirect reasoning.

In that context the average radiation values from relatively large areas and/or for a number of satellite passes are being employed; the errors or the variability of single readings therefore are of little or no consequence. These become important however when one attempts to interpret the meso-scale radiation patterns obtained for restricted areas and individual synoptic situations, either in isolation or in conjunction with satellite cloud photos. At the present state of camera resolution the interpretation of satellite photographs in terms of cloud types and heights requires a good deal of experience and subjective judgement which makes it hard to place complete confidence in the result of the analysis. It will be a very different matter once the television pictures approach the detail shown on the superb photos brought back by astronauts (cf. e.g. Conrad and Cooper, 1965). For the time being however even a slight increase in the objectivity of interpretation through the infrared radiation data could represent a substantial benefit for the meteorological understanding of events in regions poor in conventional upper air observations.

All the radiation satellites so far launched have used the TIROS II radiometer installation, and therefore any one of the available series of records is of equal value for basic study. In the present report we shall be concerned with the channel 2 data from TIROS III for the period July through August 1961 and the region of Southeast Asia. After some comments on their reduction and form of presentation, a 19-day period (August 15 to September 2, 1961) will be examined in some detail in terms of synoptic conditions

and radiation patterns, before an attempt is made to reconcile the two. Finally the possibility will be explored of utilizing the texture of the radiation surface (a new concept defined in section 7) for conclusions concerning the geometry of broken cloud patterns.

2. The Channel 2 Radiation Data Supplied by TIROS III.

Details of the TIROS radiometers and their mode of operation are given in the appropriate Users Manual (NASA 1962). For the present purpose it suffices to note the following:

a) The radiation intensity recorded for a given geographical point refers to an area not less than that of a circle with 70 km diameter and possibly as large as that of an approximate ellipse with major and minor axes of the order of 400 and 200 km, respectively, for the largest nadir angles allowed in practice before rejecting radiation observations (55° - 60°). The geometry involved is shown in Fig. 1.

b) The same geographical point supplies a number of radiation readings during a given orbit. While all these readings fall into a period which is sufficiently short for changes in meteorological conditions to be neglected they are obtained at different points of the orbit; thus they represent a range of different nadir angles and therefore also of area shapes and sizes.

c) The radiation intensity used for synoptic comparisons represents a smoothed value obtained by fitting a surface of best fit in the least square sense to all radiation readings within $2\frac{1}{2}$ degrees square influence region around the geographical point in question. The resulting smoothed radiation intensities form a $\frac{1}{2}^\circ$ latitude and longitude grid, and a variety of safeguards is applied to ensure that both the amount of information and the smoothing are adequate (Baer and Kamm, 1965). Thus the inhomogeneities listed under b) are effectively eliminated, together with any information they may contain. However, it would clearly be a simple matter to preserve and extract such information during the computer reduction of the raw radiation data and to present it alongside the smoothed radiation intensity which presently forms the only output obtained.

3. Synoptic Features of the Southeast Asia Region, August 15 - September 2, 1961.

The general area to be considered is shown in Fig. 2. Detailed radiation patterns covering part or all of the area marked

by the square for 12 orbits will be examined in the next section, but for the synoptic background the entire region covered by fig. 2 had to be studied. The meteorological information available for this purpose consisted of upper wind observations replotted without their stream line analysis from the twice daily upper air charts of the Thailand Meteorological Service.

The detailed synoptic processes of this continental tropical area are not yet well understood and are presently the subject of intensive research (cf. e.g. Riehl, 1966). This made it undesirable in the present context to attempt ambitious analyses which could but beg many of the questions the study itself was in some small way to help solve. Instead the following procedure was adopted: daily charts for each of 3 levels (700 mb, 500 mb, 200 mb) were first scrutinized independently for evidence of troughs, ridges, shearlines, and eddies. Next the reality and motion of such features was established by means of subsequent charts and checked through time cross sections for a few key stations with good observational continuity. Finally composite charts of the surviving features were constructed for the main "natural" periods defined by these features themselves.

The examination of individual charts showed that at the two lower levels invariably there was more or less definite evidence of a trough or a shear line over the Southeast Asian land mass, but little or no persistence from day to day in its position. This is illustrated by figs. 3 and 4 which show the individual troughs at the 700 and 500 mb levels for the entire period. Broken lines have been used in cases of weakly developed features.

A very different picture emerged from the analysis of the 200 mb charts (figs. 5 and 6). Here meridional troughs and ridges were the rule and these appeared to move steadily downstream in the easterly flow which prevails at high levels over this region in summer. In the north the extent and shape of these troughs and ridges were difficult to determine owing to lack of regular observations, but in the south upper winds from the Malaya Peninsula clearly showed them to become indistinct in approximately 10° latitude. This is demonstrated by the 200 mb winds in the time cross sections for Singapore (fig. 12) and Songkhla (fig. 13) where isolated changes could hardly be interpreted as due to the passage of large-scale wind field features without a knowledge of events further north.

These events are seen most clearly in the very regular series of observations for Hong Kong (fig. 7) which vary substantially in

accordance with the movement of the synoptically deduced troughs and ridges of figs. 5 and 6. For downstream developments, the winds at Saigon (fig. 9) and Bangkok (fig. 10) are most revealing; time sections for Manila (fig. 8) and Chiengmai (northern Thailand, fig. 11) have been added mainly to close the ring around the area, but Manila is somewhat too far from the mainland for a confident extrapolation across the China Sea, and the record for Chiengmai lacks the continutiy desirable for the present purpose.

In the Hong Kong winds for the 200 mb level the passage of 4 troughs and 3 ridges can be clearly identified. One of the ridges (R_3) was located above a low-level trough, and this should have facilitated tall cloud development. Two low-level disturbances in the Hong Kong time cross section appear to have either developed from above or else were independent of the upper level events; this is reminiscent of the organization of the atmosphere in lower latitudes.

The second of the Hong Kong troughs appears to have left its mark also on the Manila (fig. 8) and Saigon (fig. 9) winds while the third even appeared at Bangkok (fig. 10) and Chiengmai (fig. 11). Two of the lower level changes were felt as far south as the Malaya Peninsula (figs. 12 and 13); this area was affected early in the period by a ridge not reflected in the winds further to the north.

With all this information and the synoptic features noted from the individual charts it is possible to construct composite pictures of two sequences of events within the period considered. The first sequence (fig. 14) extended from August 15 to August 24 and involved the passage of two 200 mb troughs and ridges over the Southeast Asia area, with orientations generally from northwest to southeast. The second ridge appears to have amalgamated with the first on August 22. In the same sub-period a cyclonic eddy came into being in the lower troposphere; this was clearly noticeable at both 700 and 500 mb on August 18 and during the following 4 days moved to the region of Chiengmai where it brought about marked wind changes up to the 500 mb level on August 22 (fig 11). The passage of the associated trough was felt as far south as Singapore, but took a more spectacular form in the strong winds over Saigon and Bangkok (figs. 9 and 10).

During the second sub-period (fig. 15) the 200 mb troughs and ridges were oriented in a northeast-southwest direction. The first system (no. 3) reached the south coast of Southeast Asia but was somewhat difficult to locate in the Manila winds. At lower levels

a cyclonic disturbance was hinted at by the Philippine Is. winds on August 23; it is not clear whether this became the 700 mb circulation south of Formosa on August 24. Subsequently this cyclonic eddy extended to the 500 mb level below a 200 mb ridge and moved in a northwesterly direction over China, while the ridge (R_3) and the associated lowlevel trough passed over Southeast Asia between August 24 and 26. Part of this development has been carefully analysed in terms of vorticity advection and vertical velocity fields by Figgins (1965). The 200 mb ridge became difficult to trace synoptically after August 26 at lower levels. Anticyclonic circulations appeared to have moved slowly in a southwesterly direction across the southern part of the region during the closing days of the period, from August 27 to September 2; this is shown also by the Songkhla winds (fig. 13).

Apart from these systems the individual charts suggested other possible disturbances, and it is clear that a more painstaking analysis would have produced rather more complicated pictures than figs. 14 and 15. On the other hand their details would have become increasingly speculative. For the present purpose the two composite charts provide a minimum of synoptic features which might be expected to have left their mark on the infrared radiation patterns for the period. These will not be examined.

4. The Satellite Cloud and Radiation Data for Southeast Asia, August 15 -- September 2, 1961.

During the period in question, twelve orbits of TIROS III provided usable radiation data for the area of interest and thirteen gave photos from which cloud mosaics could be constructed. Details of these orbits and the areas covered are given in table 1. For seven passes, both mosaics and radiation data are available, but three of these missed most of the study area. Radiation intensity isopleths were drawn for each pass and for the area of the rectangle in fig. 2, with 0.05 ly min $^{-1}$ spacing. The recorded intensities ranged from as low as 0.16 ly min^{-1} to 0.61 ly min^{-1}, correspondingly to black body temperatures of 211K and 295K, respectively. In the mean tropical atmosphere these temperatures occur near the 160 mb and 800 mb levels, but allowance must be made in this connection for the systematic differences between actual and effective (radiation) temperatures (cf. fig. 26 and section 7).

The radiation charts for the period under consideration do not show the systematic differences between land and sea areas

established for the pre-monsoon period by Saha (1966) from a somewhat larger material of TIROS IV data. Typical of the present charts, and perhaps of the monsoon period, is that for August 16 (figs. 16 and 29) in which a band of low and high intensities extended across the Southeast Asian land mass into the South China Sea and another ran across Sumatra and the Malaya Peninsula into the Gulf of Siam.

Not only the arrangement but also the scale of the cold and warm areas in figs. 16 and 29 was fairly representative of the radiation charts in the period here considered. Occasionally however larger features were suggested. An example was the last radiation chart of the series (September 1, fig. 25) in which a warm and a cold region extended side by side in a straight line all the way from Sumatra to beyond Hong Kong. The synoptic basis of such a pattern should be discernible even with the sketchy station network of this area, and we turn now to a collation of the radiation charts with the synoptic information of section 3.

Table 1: TIROS III Cloud and Channel 2 Radiation Runs Over Southeast
Asia, August 15 - September 2, 1961

Date	Local Time	Orbit No.	Mosaic	Radiation	Cover and Quality of Photos	
Aug.	hours G					
16	15	500/501	X	X	complete,	good
17	14.30	514/515	X	-	NW missing,	good
18	14	528/529	X	-	NW missing,	good
18	15.30	529/530	X	-	outside area,	good
19	13	542/543	X	-	east of area,	good
19	15	544	-	X	northern half only,	good
20	12	557	X	-	east of area,	good
20	14	558	X	-	northern extreme only,	good
22	00	579	-	X	Malay Peninsula only	
23	12	600	X	X	NE corner of area only,	good
24	00	607	-	X	Western half of area only	
24	12	614	X	X	complete,	good
25	11.30	628	X	X	complete, medium quality	
26	11	642	-	X	South China Sea only	
28	10	669/670	X	-	complete,	good
28	11.30	671	X	X	east of area	
29	11	685	X	-	NW corner only,	poor
31	10	713	-	X	SE corner only	
Sept.						
1	9	727	-	X	SE corner only	

5. Synoptic Discussion of Radiation Data.

In this section the main warm and cold areas of the radiation charts are placed in relation to the noteworthy synoptic features at the 700, 500, and 200 mb levels. Some of these are labelled in the terms of figs. 14 and 15; the remainder must be given somewhat less weight as not clearly discernible on subsequent or preceding charts.

August 16, (fig. 16b) The cold area over central Southeast Asia coincided with a cyclonic eddy at the 500 mb level. The main shearlines both at 700 and 500 mb agreed with the position of the field over the South China Sea but over Southeast Asia had a north-westerly trend whereas the main low temperature band on the radiation chart continued in a southwesterly direction, along the 200 mb trough. This included hints of a closed circulation over the Gulf of Siam. The cold area near Hong Kong was not far from an anticyclonic eddy at the 700 mb level. All the cold regions correlated well with dense cloud masses in the TIROS III photos, but high temperatures were suggested for some regions with appreciable cloud cover. Thus the cloud patch south of the southern tip of Vietnam extended well inland to the north whereas the radia-tion chart shows a closed cold region over the sea only. Again, the coast along the Gulf of Tonkin stood out clearly as a boundary between scattered cloud on the land and apparently clear skies over the sea, whereas the radiation chart shows rather high temperatures for the entire area.

August 19, (fig. 17) The radiation chart was restricted to the northern parts of Southeast Asia where moderately low tempera-tures occurred in the region of the 700 mb trough. A warm area just north of Hainan Island coincided with the 200 mb trough T1. The cyclonic eddy over the South China Sea was outside the radiation chart area but the cloud mosaic showed an extensive cloud cover there. A weekly spiraling cloud mass near Formosa occurred near an anticyclonic eddy at the 500 mb level.

August 23, (fig. 18) The radiation chart showed a belt of low temperatures along the 700 mb and 500 mb troughs from the South China Sea in a northwesterly direction. An area of very low radiation intensities near Hainan Island coincided with a suspected cyclonic circulation in the 200 mb trough T3 but could also be accounted for by a slight extension of a low-level trough. It is of interest that high temperatures over the Malaya Peninsula persisted in the next radiation chart which was obtained at local midnight but unfortunately did not cover the area further to the east.

August 24, (fig. 19) Low radiation values were recorded from an extensive cloud area south of Hong Kong in the region of the 700 mb and 500 mb troughs. The position of the latter over South Vietnam and Cambodia was in better agreement than the more northerly position of the 700 mb trough with an extensive low temperature band in the radiation chart and with the cloud areas of the mosaic over the southern coast of Southeast Asia.

August 25, (fig. 20) The radiation chart had a warm belt along the 700 mb trough and a distinct cold patch further south where a cyclonic eddy had been suspected at the 500 mb level. Otherwise it is very noticeable in this case that the radiation pattern had a distinctly finer scale than the synoptic features deduced by inspection.

August 26, (fig. 21) The lowest radiation intensities of the entire series occurred in the region of the mid-tropospheric eddy near Hong Kong, and another cold region was indicated near the southern tip of Southeast Asia not far from the 500 mb trough.

August 28 and 29 (figs. 22 and 23) Extensive low radiation areas over Southeast Asia had no clear connection with the large-scale synoptic features standing out on casual inspection, with the exception of the cyclonic eddy at the 500 mb level over Hainan Island.

August 31 and September 1, (figs. 24 and 25) On the first of these dates the low-radiation areas were in excellent agreement with the positions of the 700 mb and 500 mb troughs, but on the following day a position not unlike that of August 16 (fig. .16) had arisen, with the troughs trending to the Northwest over Southeast Asia and the low-radiation area continuing in a southwesterly direction towards Sumatra. A tentative explanation of this and similar patterns would be that the low temperature regions represent vast sheets of dense cirrus moving with the flow at the 200 mb level away from regions of active convection near the low-level troughs. It is common for jet aircraft to spend periods of the order of an hour flying through cirrus of this type, so that the size of the low radiation areas on the charts here presented is not incompatible with this interpretation.

Summing up the foregoing discussion, in general it does not appear to be difficult to find some synoptic or other meteorological reason for low radiation intensities. One striking feature is that

the low temperatures in question permit no immediate conclusion as to the level of the synoptic feature possibly responsible. Thus the lowest temperatures in the entire series occurred near the deep vortex of August 26, but radiation intensities only a little higher were found over the South China Sea on August 31 when there was only a 700 mb shear line around to explain them. Clearly, since even a convergence line at very low levels can be associated with cb clouds and extensive cirrus sheets, only the most complete and accurate description of the three-dimensional velocity field could conceivably explain minor details of the radiation patterns, to the extent that these really reflect different cloud heights (cf. section 7). Conversely, the precise flow field information that can be derived from the magnitude of the smoothed infrared radiation values alone must be severely limited.

There exists however a more direct link between cloud scale and precipitation, and it seems possible that despite their smoothed nature the radiation intensities here considered might reveal the greater height of cb clouds associated with heavy rain. This question will be briefly examined in the next section.

6. Radiation Intensities of Heavy Rain Areas.

To examine the radiation emitted by areas with heavy rain it is necessary to have pluviograph data from which the time of occurrence of the rainfall can be pinpointed and placed in relation to that of the satellite pass. A great deal of such observations exists for the Southeast Asian area where they are obtained as part of the Mekong River Project. For the present investigation all available pluviograph records were scrutinized for 22 days in July and August 1961 for which TIROS III radiation values had been obtained and evaluated. Heavy rains were defined as having exceeded 10 mm hour^{-1}. In most cases maximum intensities were considerably higher and occurred during a rainy period lasting several hours. The hour of the heaviest rain was then chosen to represent the occasion in question.

A tendency for especially low radiation intensities to be recorded from such heavy rain areas can be established by comparing their radiation values for different time intervals between the rain occurrence and the passage of the satellite. Since groups of cb clouds have life spans of the order of at least several hours a precise coincidence of the rain with the radiation minimum would not be expected to happen. In fact the radiation minimum might well occur

during the decay stage of the cloud, as its dense cirrus shield spreads out downwind at the 200 mb or even higher levels. Thus for equal positive and negative time lag between the rain and the radiation measurement lower temperatures would be expected after than before the rain. With increasing time lag the radiation intensity should slowly approach a somewhat higher mean value representing the usual mixture of average size clouds and clear sky typical of tropical regions.

For the present material table 2 shows the mean radiation intensities for areas of heavy rain falls which occurred at different time lags from a satellite pass. The standard deviations of the first two group means have been included to enable the significance of their difference to be assessed.

Table 2: Mean Radiation Intensities (ly min^{-1}) Recorded by TIROS III for Areas of Heavy Rain (10 mm hour^{-1}) at Different Time Lags Between the Rain and the Satellite Pass over the Mekong River Basin, July/August, 1961.

Time lag, hours satellite passed	1	2-3	4-5	6-7	8-9	10
After rain	0.326	0.343	0.343	0.316	0.331	0.327
No. of cases	21	12	8	15	11	8
Before rain	0.329	0.391	0.369	0.378	0.371	0.362
No. of cases	15	14	18	13	8	15
Mean	0.327	0.369	0.360	0.345	0.367	0.351
No. of cases	36	26	26	28	19	23
Standard deviation of mean	0.012	0.017				

The most striking features of table 2 is the consistently lower radiation intensities recorded from rain areas after the time of the most intense precipitation. Within a period of approximately one hour on either side of the satellite pass the intensities are equal and

somewhat lower than those at slightly larger time lags, but the main effect is the expected one of a slight lowering in radiation intensity subsequent to heavy rain and presumably due to the development of cirrus shields close to the rain area.

This effect can even be demonstrated for an individual occasion. Table 3 refers to August 23 when two radiation runs followed one another within 12 hours of one another (orbits 600 and 700):

Table 3: Rainfall Amounts and Radiation Intensities for all Southeast Asian Stations in the Overlap Region of Orbits 600 and 700 of TIROS III, August 23, 1961.

Station	Kompong Cham	Svarieng	Saigon	Bara	Surin
Rainfall (mm)	18.3	13.4	20.1	7.0	14.6
Period (hours G)	23-24	20-21	17-18	17-18	21-22
Channel 2 radiation					
ly/min 12G	0.39	0.44	0.46	0.42	0.39
24G	0.28	0.29	0.30	0.30	0.29

Any satisfaction that might perhaps be derived from this small advance in the interpretation of a minima in satellite radiation intensities must however be offset by a realization of how much remains to be explained for intermediate intensities. From what was said in section 2 it is clear that these often may not have any unique explanation at all since even the smallest area viewed by the TIROS radiometers is large enough to enclose a variety of clouds or groups and streets of clouds. Especially over the tropical oceans the sizes, heights, and arrangements of cumuli are very closely determined by the large-scale flow field (Malkus and Riehl, 1964). The detection of these details is therefore of crucial importance, yet on the basis of the present satellite photo resolution remains largely a subjective exercise in ingenuity. It will now be shown, however, that the satellite radiation data offer a new inroad to this problem.

7. The Texture of the Radiation Surface and its Meteorological Significance.

The smoothing of the raw radiation data is an essential prerequisite for their synoptic interpretation but obliterates a good deal of the information contained in individual radiation swathes (cf. e.g. Chu and Spar, 1964), let alone the original analogue traces before they have been digitized at the standard 0.1309 sec. intervals which is standard for this computer operation (Bandeen, Kunde, Nordberg, and Thompson, 1964). Study of the analogue traces is believed to make it possible to discern even individual large clouds, but clearly the effort involved in such an analysis makes it impractical for synoptic studies (except those in which a very restricted area such as that occupied by a growing hurricane is of principal interest).

For synoptic-scale studies the question arises whether some of the information obliterated in the smoothing of the radiation surface could perhaps be retained and used to describe what might be termed its "texture." Analogy with the way the texture of a material is determined by visual means at once suggests both a definition for this new concept and a simple way of measuring it; viz. in terms of the radiation intensities emitted from the same geographical area under different nadir and azimuth angles. A smooth surface would be one showing little or no change in radiation intensity with these angles whereas a highly textured surface the radiation intensity would depend very much on the angles under which the surface is viewed by the satellite.

The change in radiation intensity with nadir angle has been discussed in the literature in terms of what is known as "limb darkening" (cf. e.g. Wark, Yamamoto, and Lienesch, 1962). In the case of channel 2 radiation this arises from the residual absorption and emission by the atmospheric gases in the window region and their increases with air mass penetrated by the radiation. According to Wark et.al. (1962) limb darkening in the channel 2 part of the spectrum is negligible for nadir angles up to 30 degrees, and even for angles as large as 60 degrees the temperature errors introduced by this effect remain below 4° C in a tropical atmosphere, the most severe case. This is demonstrated by fig. 26 which has been adapted from figs. 9a and b of the paper by Wark et.al. (1962) and the fact, revealed by their examination of 106 model atmospheres (see fig. 4 of their paper), that the maximum limb darkening is 3 times as strong for a nadir angle of 78.5° as for 60°.

In comparison with the synoptically observed radiation temperature <u>differences</u> therefore the limb darkening effect in channel 2 radiation can therefore safely be disregarded. However, there exists another directional effect which was mentioned but not pursued by Wark, Yamamoto, and Lienesch (1962). This arises from the change in proportion of cloud and ground surfaces seen by the radiometer with different nadir angles, when a broken cloud pattern is present. It will now be shown by a simple geometrical argument that such cloud patterns give rise to much larger changes in radiation intensity with nadir angle than those established for limb darkening by fig. 26.

Fig. 27 shows a schematic representation of a small area in a field of cumulus clouds. Over a real cloud area viewed by the satellite radiometer the various geometric parameters describing such an arrangement will have a range of values but for the argument that follows it is adequate to regard the arrangement of fig. 27 as the average "unit cell" of the cloud pattern. A degree of generalization will be introduced in the algebra by allowing the two "clouds" to have different heights h and h' (the latter cloud being nearer to the satellite), and evidently it would not be difficult to permit different diameters and a variety of cross section shapes in place of the squares assumed in fig. 27.

To determine the mean temperature of the unit area as seen from above by the satellite under a zenith angle β two ranges of that angle must be distinguished, viz. those for which the ground surface is visible and those for which the entire view field is filled by cloud walls and tops. The boundary between the two ranges is defined by

$$\beta = \beta_L \equiv \tan^{-1} \left(\frac{s}{h'}\right) \tag{1}$$

This follows from the fact that the portion of the cloud wall invisible to the satellite, z, is determined by the relation

$$(h-z)/(h'-h) = \frac{s-(h'-h)\tan\beta}{(h'-h)\tan\beta}$$

so that

$$z = h' - \frac{s}{\tan\beta}$$

For a given zenith angle β the projections of the different distances or areas in fig. 27 are as follows:

1. cloud top (temperature T_2): $d \cos \beta$

2. cloud wall: assuming a linear temperature change with height, its mean temperature for $z = 0$ or $\tan \beta \leq s/h'$ is $(T_1 + T_2)/2$ but when only part of the wall is visible to the satellite this becomes instead

   $\frac{1}{2} [T_1 - (T_1 - T_2) z/h + T_2]$. The projected area is

   $(h-z) \sin \beta$.

3. ground surface (temperature T_0): $s \cos \beta - h' \sin \beta$.

The mean temperature of the area element can now be written down for the two cases $\tan \beta < \tan \beta_L = s/h'$ and $\tan \beta \geq s/h'$:

a) $\beta < \beta_L$ ground visible, $z = 0$:

$$\overline{T} = [T_2 \, d \cos \beta + (T_1 + T_2)/2 \, h \sin \alpha + T_0 \, (s \cos \beta - h' \sin \beta)]/(d+s) \cos \beta$$

$$= \frac{T_2}{d+s} (d + \frac{h}{2} \tan \beta) + \frac{T_1}{2(d+s)} \, h \tan \beta + \frac{T_0}{d+s} (s - h' \tan \beta) \tag{2}$$

b) $\beta \geq \beta_L$ ground invisible, $z > 0$:

$$\overline{T} = T_2 \frac{d}{d-s} + \frac{\tan \beta}{2h(d+s)} [T_1 (h-z)^2 + T_2 (h-z)(h+z)]$$

$$= \frac{T_2 d}{d+s} - \frac{\tan \beta}{2h(d+s)} [T_1 (h-h')^2 + T_2 (h^2 - h'^2)] + \frac{s^2}{2h(d+s)\tan \beta} (T_1 - T_2) +$$

$$+ \frac{s}{h(d+s)} [T_1 (h-h') + T_2 h'] \tag{3}$$

A check on these results can be made by putting $\beta = \beta_L$; this renders (2) and (3) identical.

For a first numerical evaluation of (2) and (3) it will be convenient and permissible to introduce non-dimensional variables for the cloud diameter and spacing in terms of the cloud height

which moreover will be assumed equal for the two clouds of the cell; thus we shall assume h = h' and

$$s = Sh \qquad\qquad d = Dh$$

where S and D are constants. The mean cloudiness is C = D/(D+S), and equations (2) and (3) take the simpler forms

$$\overline{T}'_{\beta < \beta_L} = \frac{DT_2 + ST_0}{D + S} + (T_1 + T_2 - 2T_0)\frac{\tan\beta}{2(D+S)} \qquad (2')$$

and

$$\overline{T}_{\beta \geq \beta_L} = T_2 + (T_1 - T_2)\frac{s^2}{2h\,(D+S)\,\tan\beta} \qquad (3')$$

The ground and cloud base temperature will be assumed constant, T_0 = 26°C and T_1 = 22.5°C, corresponding to the surface and 1 km levels in the mean tropical atmosphere. The cloud top temperature T_2 will be set equal to that of a rising bubble of surface air after isothermal expansion to 960 mb and addition of 1.5 g/kg of moisture (cf. Riehl, 1954, table 11.8). This yields the temperatures shown in table 4:

Table 4: Assumed Cloud Top Temperatures (after Riehl 1954).

Height of cloud h (km)	1	2	4	8	12
Height of cloud top (km)	2	3	5	9	15
Approximate pressure level mb	800	700	500	300	200
Temperature T_2 °C	18	12	0	-26	-50

The calculations have been made by slide rule for the following cloud patterns:

	Diameter		Spacing		Mean Cloudiness	
1.	D	0.5	S	1.5	C	0.25
2.	D	0.5	S	0.5	C	0.50
3.	D	0.75	S	0.25	C	0.75

The results of the calculations are shown in the top part of fig. 28, with the cloud top temperature T_2 as ordinate and the zenith angle β as abscissa; an approximate nadir angle scale has been added, using the average satellite height H=716 km in the equation

$$a = \sin^{-1} (\frac{R}{R+H)}^2 \sin \beta.$$

Fig. 28 suggests that the radiation temperature of broken cloud areas will change most in the region where limb darkening effects are entirely negligible, i.e. for small nadir angles, and that the changes will be very substantial for large clouds. The change in the shape of the "texture" curves with mean cloudiness, from convex to concave curvature, should also be noted. All these features provide a basis for assigning a mean cloud top height and mean cloudiness to observed radiation intensities recorded from a given area under different nadir angles.

It will clearly be a simple matter to evaluate equations (2) and (3) in much more detail by computer for any desired cloud arrangement or in terms of probability distribution of cloud size, spacing, and height. The observed cloud distributions described and analysed by Malkus and Riehl (1964) offer especially interesting possibilities in this connection. To wind up the present discussion, however, it would be helpful to confirm the existence of the suspected radiation surface texture from actual satellite data.

The only readily available material for this purpose was a partial listing of the radiation readings for orbit 501 (August 16, 1961). The detailed intensity contours of the radiation surface for this occasion are shown in fig. 29 but the corresponding cloud mosaic was used to select the four test areas marked by different hatching in fig. 29 as given in table 5:

Table 5: Areas Tested for Radiation Surface Texture, Orbit 501,
TIROS III, August 16, 1961.

Area No.	Longitude Ranges ° E	Latitude Ranges°E	Description of Cloud Cover (Neph Analysis)
1	102 - 105	12 - 15	Dense cb
	107 - 108	15 - 17	
2	103 - 105	15 - 20	Broken cb
3	100 - 103	10 - 11	Largely clear with iso-lated cloud patches
4	106 - 107	18 - 20	
	108 - 110	16 - 18	Cloudless ocean areas
	107 - 108	17 - 18	

Fig. 30 shows the available individual radiation intensity
values for these four areas plotted against their nadir angles. In
judging the result it is important to remember that the location of
the point viewed by the radiometers is not precisely known; more-
over, the nature of the cloud distribution of August 16 made it
difficult to delineate sufficiently large areas of contrasting cloudiness.
Nevertheless fig. 30 clearly shows the expected features. Areas 1
and 4 show no change in radiation intensity for widely different nadir
angles whereas changes in intensity are apparent for area 2 and, to
a lesser extent, area 3. The shape of the area 2 curve suggests a
lower mean cloudiness than that of the area 3 curve, but a larger
number of individual intensities as well as a greater variety of
nadir angles would be required to confirm this difference and to
determine the average cloud height by comparison with the curves
in fig. 28 or a more sophisticated texture nomogram.

8. Conclusions.

It has been shown in this report that apart from suggesting
minimum radiation temperatures for the regions where these would
be expected to occur on synoptic grounds the smooth surfaces con-
structed from satellite radiation readings have a "texture" which
is related to the geometry of broken cloud regions emitting

intermediate radiation intensities. A full substantiation of this result will require the examination of a large number of radiation surfaces; it is suggested that future calculations of these surfaces should retain and exhibit, in some convenient form, what has here been termed their texture - the local change in radiation intensity with nadir angle. The possibility of additional texture-like effects from changes in azimuth (possibly in relation to that of the sun) must also be explored. There seems a good chance that the study of these effects for different cloud patterns will show that the regions of intermediate radiation intensities, so far completely disregarded, provide important clues to the meteorological conditions, especially in tropical regions where broken cumulus clouds of widely varying sizes and heights predominate.

Acknowledgements

References.

Bandeen, W.R., Kunde, V,, Nordberg, W., and Thompson, H.P.
    1964. TIROS III meteorological satellite observations of a
    tropical hurricane. Tellus 16, 480-502.

Chu, R.T.P., and Spar, J. 1964. A TIROS III view of hurricane
    Betsy. Geofisica Internacional 4, 247-262.

Conrad, P., and Cooper, G. 1965. The earth from Gemini 5.
    Life 59, No. 13 (September 24, 1965), 30-39 and title page.

Figgins, E.D. 1965. Weather pattern recognition from TIROS
    pictures over Southeast Asia. M.Sc. thesis, Colorado State
    University.

Malkus, Joanne Star and Riehl, H. 1964. Cloud structure and distri-
    butions over the tropical Pacific Ocean. University of California
    Press.

Möller, F. 1962. Some preliminary evaluations of TIROS II radiation
    measurements. Archiv für Meteorologie, Geophysik, und
    Bioklimatologie Ser. B 12, 78-94.

National Aernoautics and Space Administration 1962, TIROS III radia-
    tion data user's manual. Goddard Space Flight Center, Greenbelt,
    Maryland.

Riehl, H. 1954. Tropical Meteorology. Mc Graw-Hill

Riehl, H. 1966. Southeast Asia monsoon study. Second Tec. Rep.
    Contract DA-28-043-AMC-01303(E). Proj. No. 28043-MC-00813(E).

Saha, K.R. 1966. A contribution to the study of convection patterns
    in the equatorial trough zone using TIROS IV radiation data.
    Tech. Rep. 74, Dept. of Atmos. Sci., Colorado State Univ.

Wark, D.Q., Yamamoto, G., and Lienesch, J.H. 1962. Methods
    of estimating infrared flux and surface temperature from
    meteorological satellites. J. Atm. Sci. 19, 369-384.

Fig. 2   Southeast Asia and area covered by radiation surface.

$\mathcal{L}$ = NADIR ANGLE
H = SATELLITE HEIGHT (720–800 km)
R = 6370 km
β = ZENITH ANGLE

$$\sin\beta = \frac{R+H}{H}\sin\mathcal{L}$$

$$L = (R+H)(\cos\mathcal{L} - \sqrt{(R/R+H)^2 - \sin^2\mathcal{L}}\,)$$

RADIOMETER VIEWFIELD (5°)
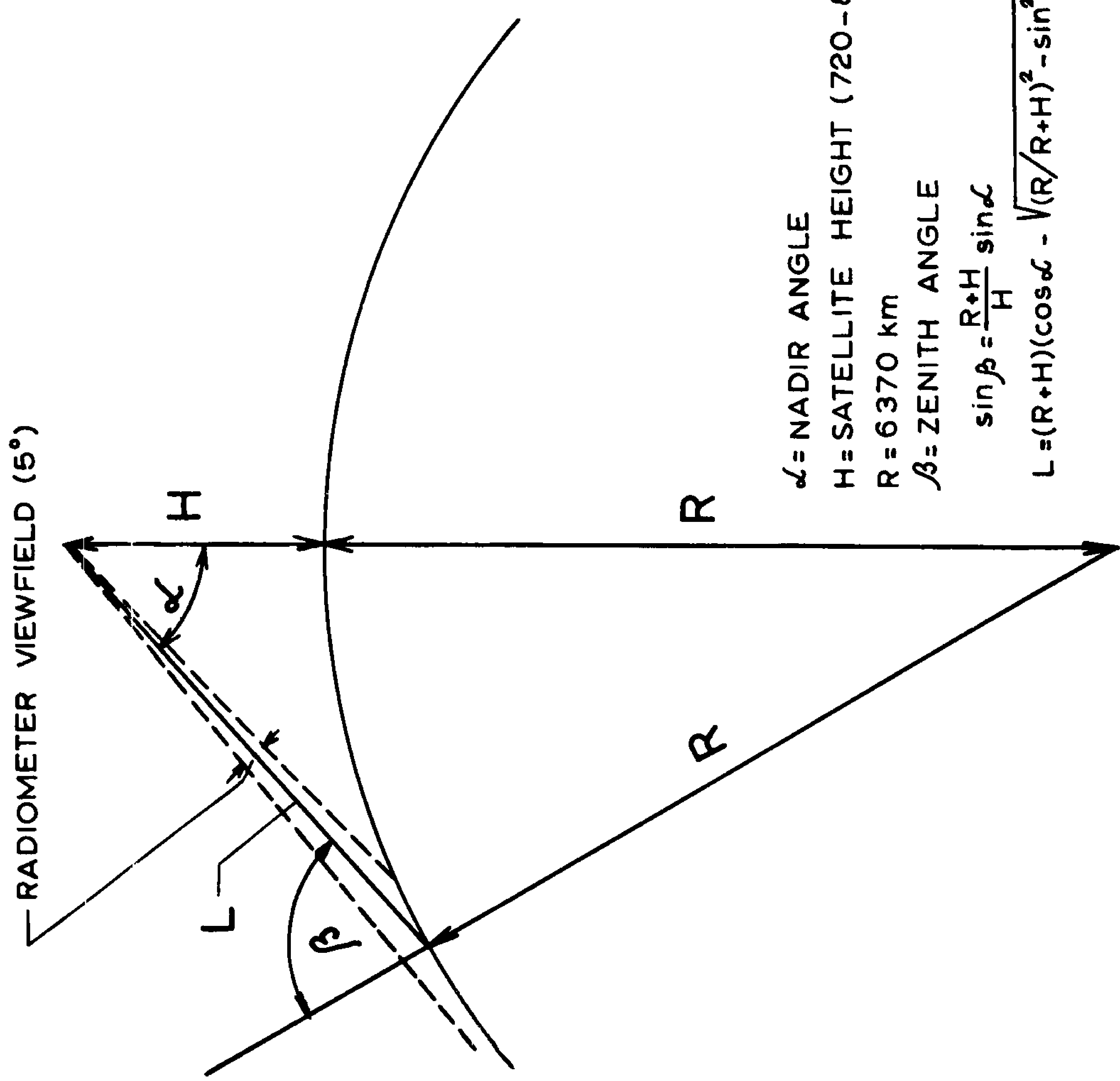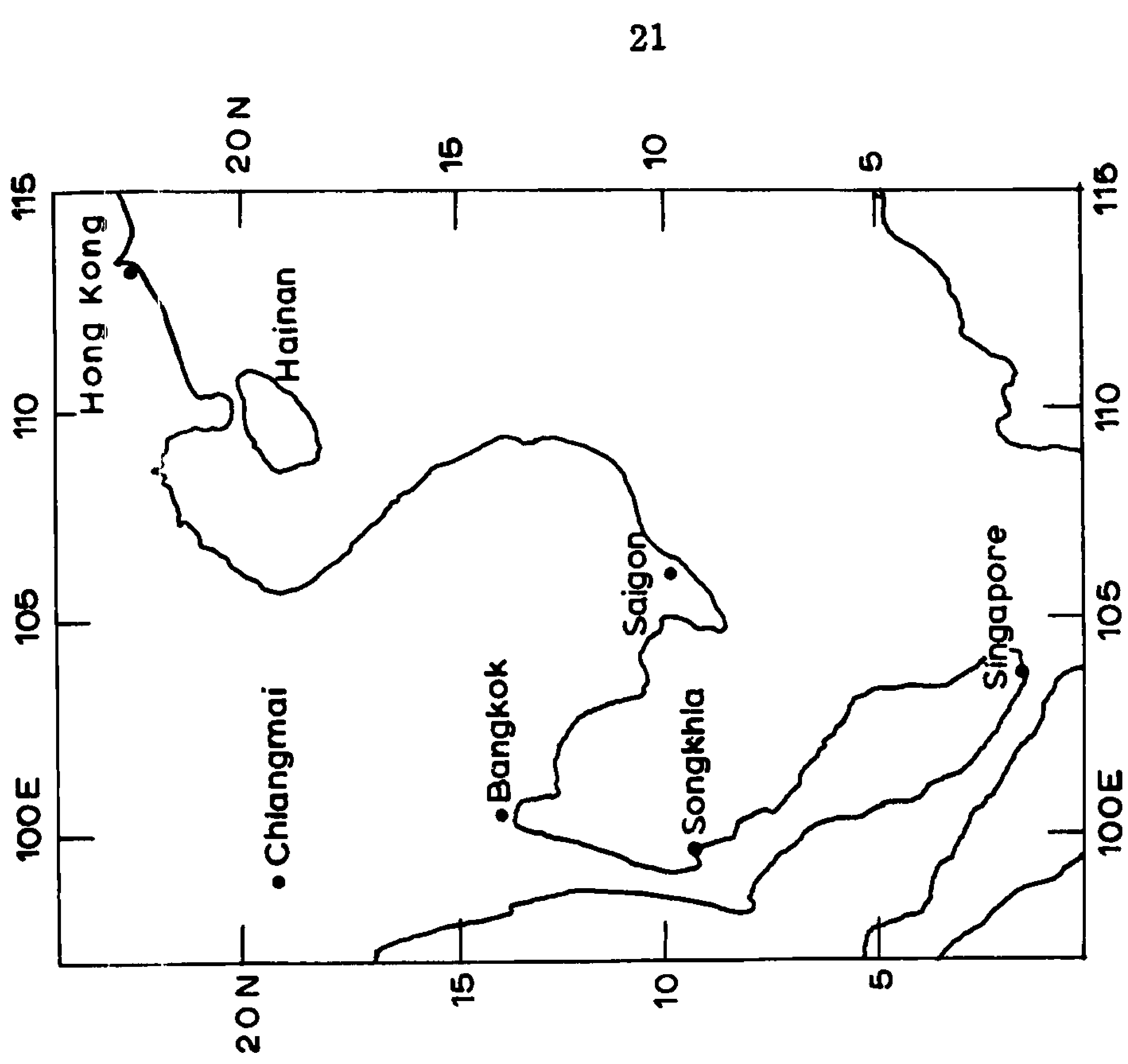
Fig. 1   Geometry of radiation measurements.
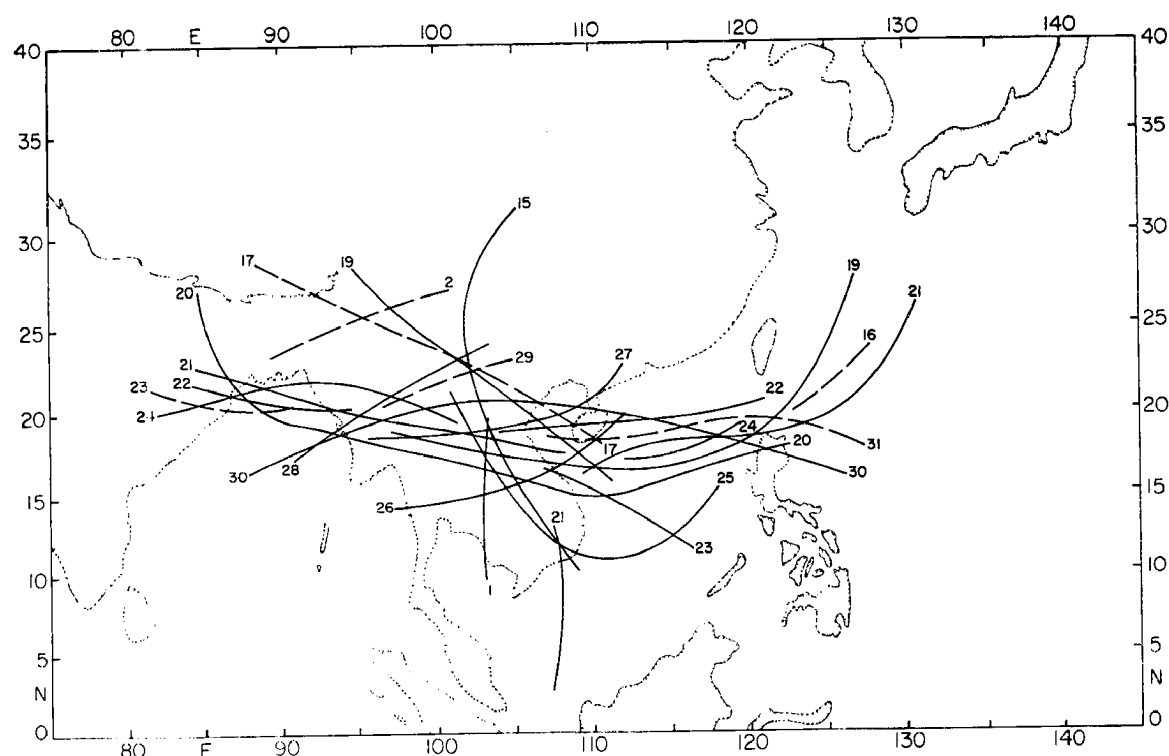
Fig. 3 Daily 700 mb troughs. Numbers are dates in August and
September, 1961.
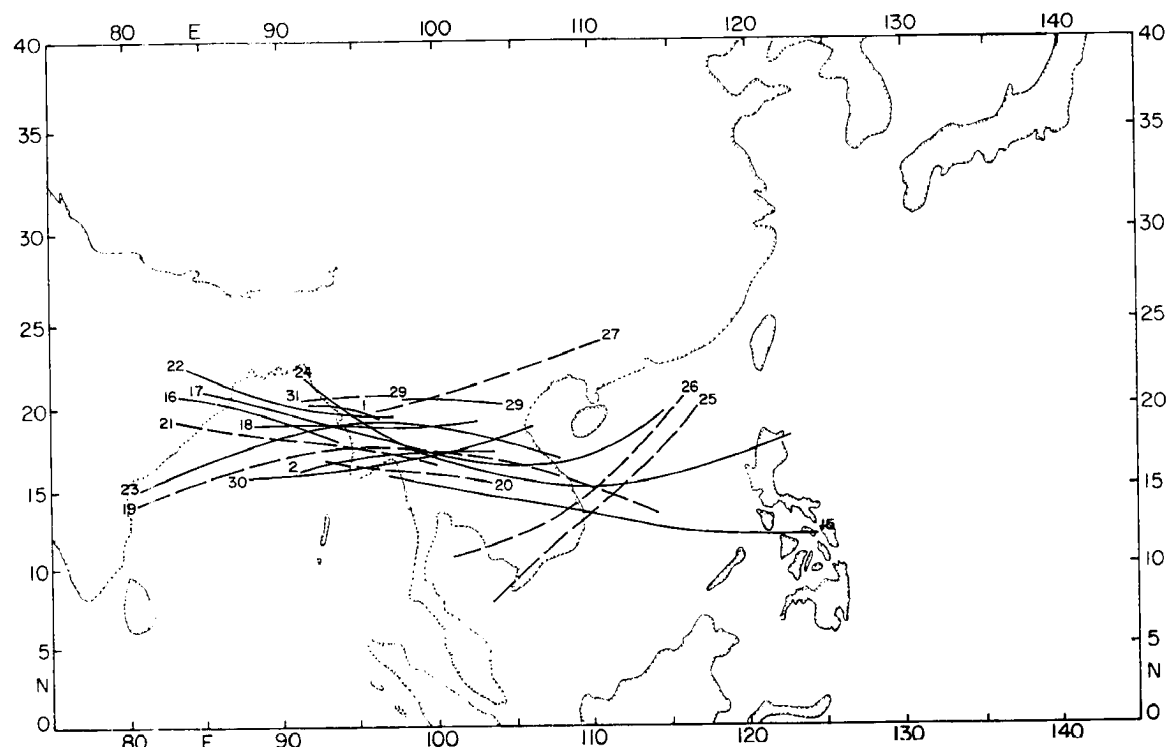
Fig. 4 Daily 500 mb troughs. Numbers are dates in August and
September, 1961.
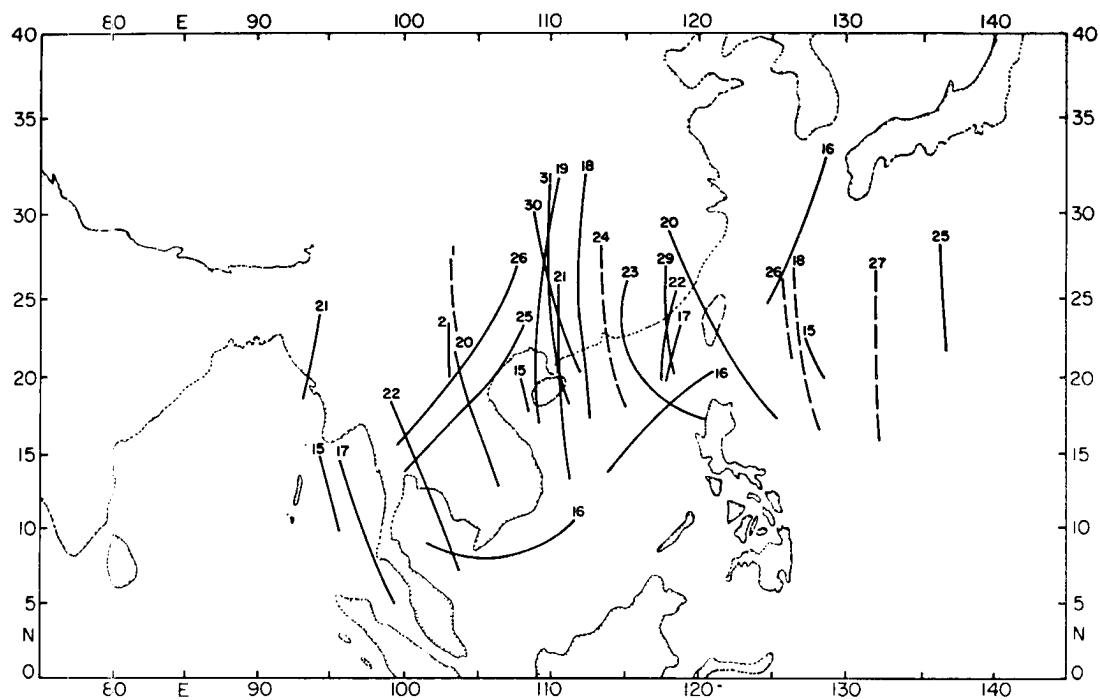
Fig. 5   Daily 200 mb troughs.   Numbers are dates in August and
September, 1961
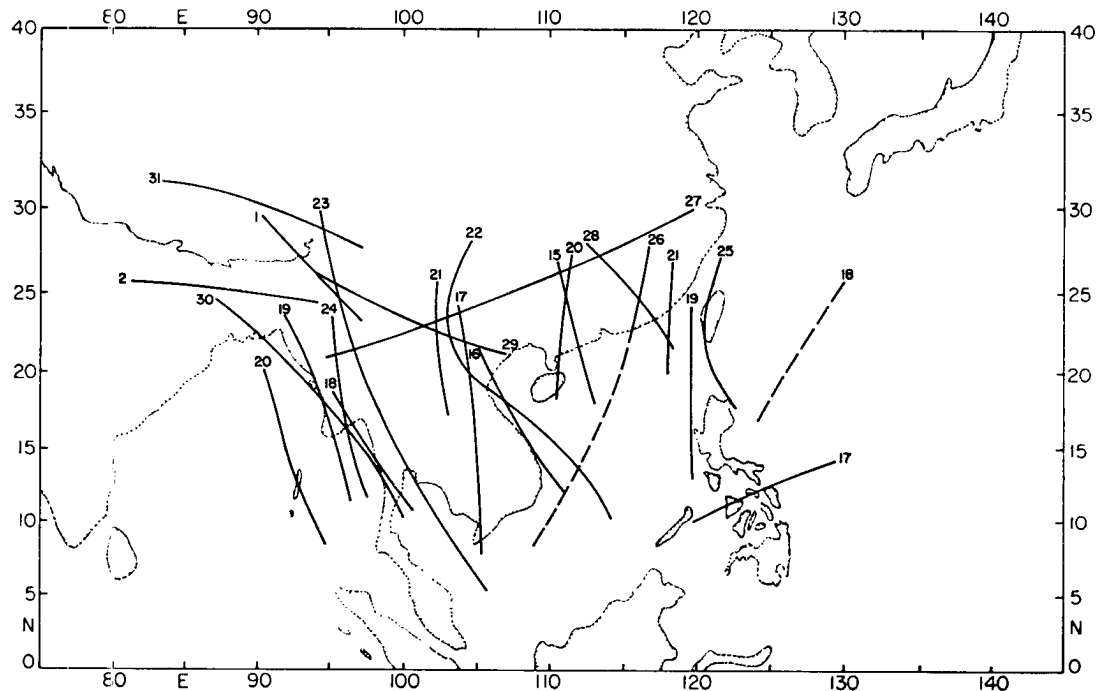
Fig. 6   Daily 100 mb ridges.   Numbers are dates in August and
September, 1961.
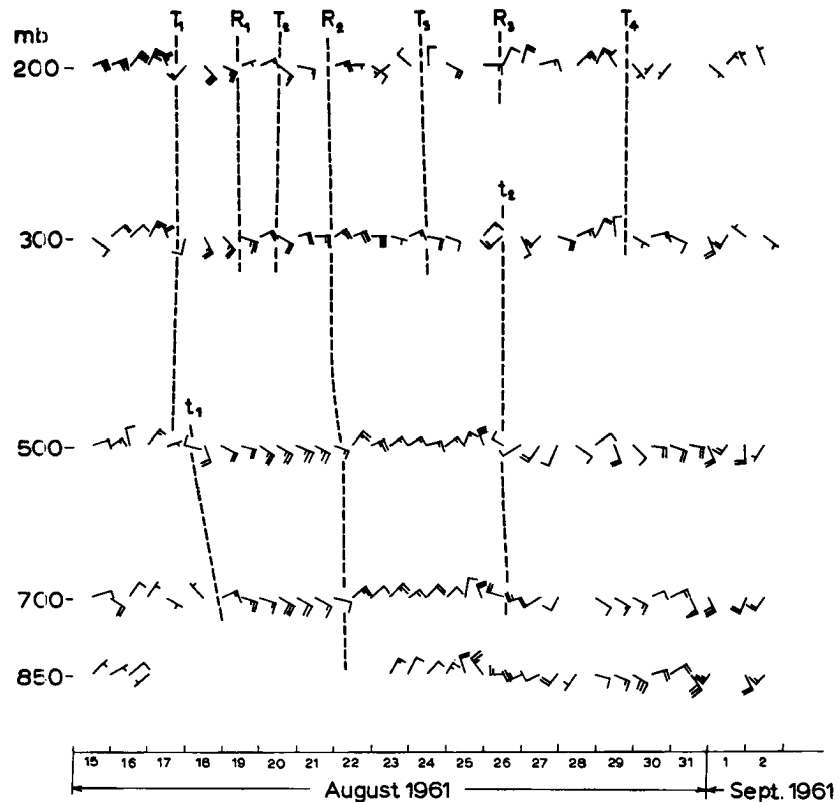
Fig. 7   Upper winds, Hong Kong.
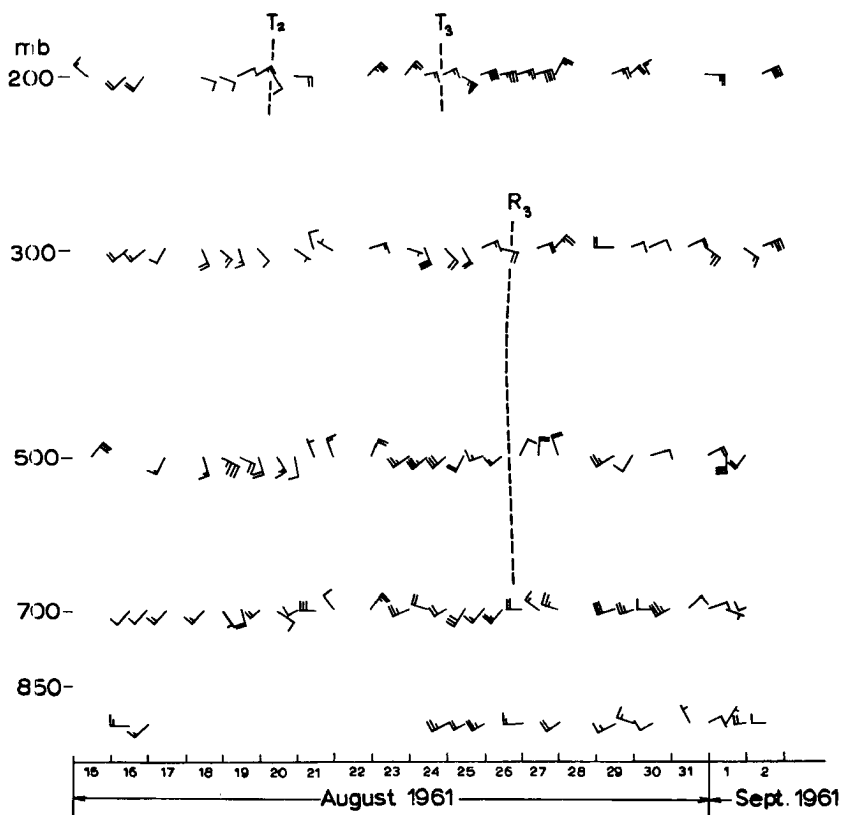
Fig. 8   Upper winds, Clark AB.
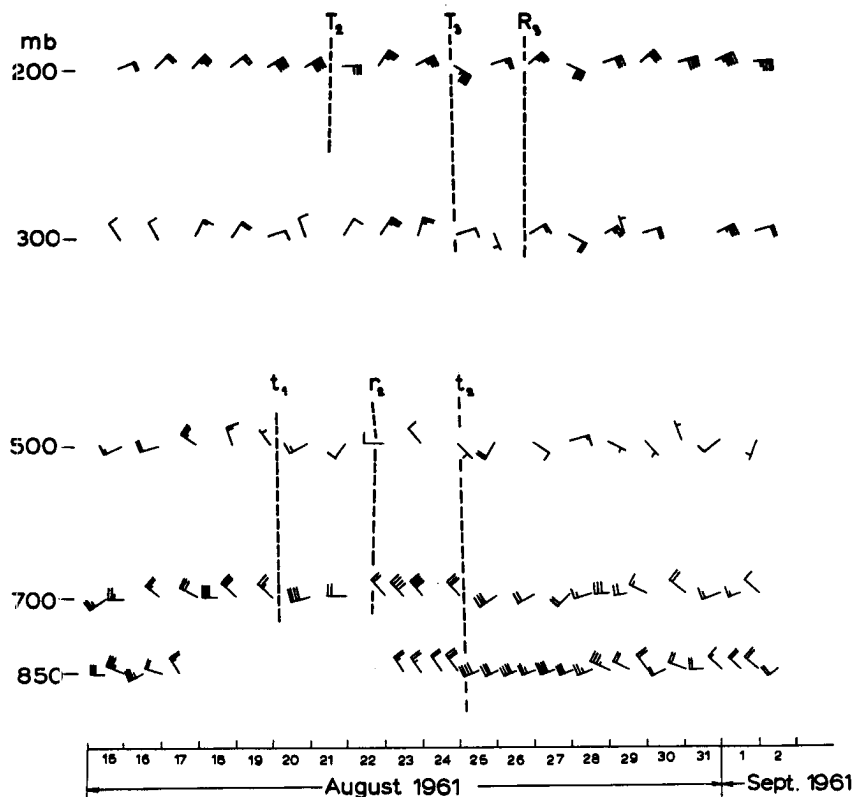
Fig. 9   Upper winds, Saigon.
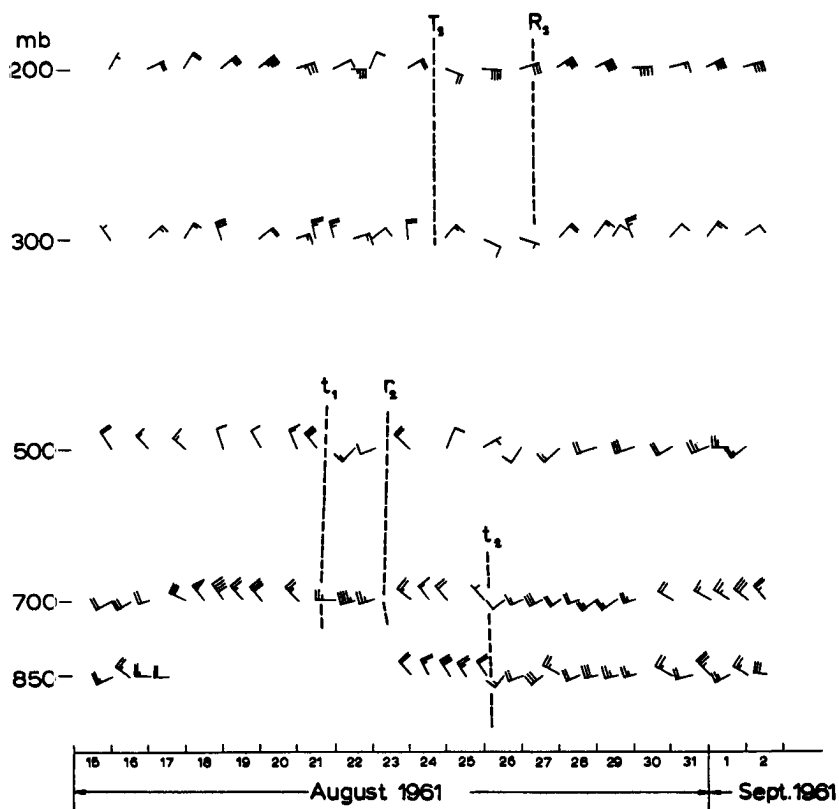
Fig. 10   Upper winds, Bangkok.
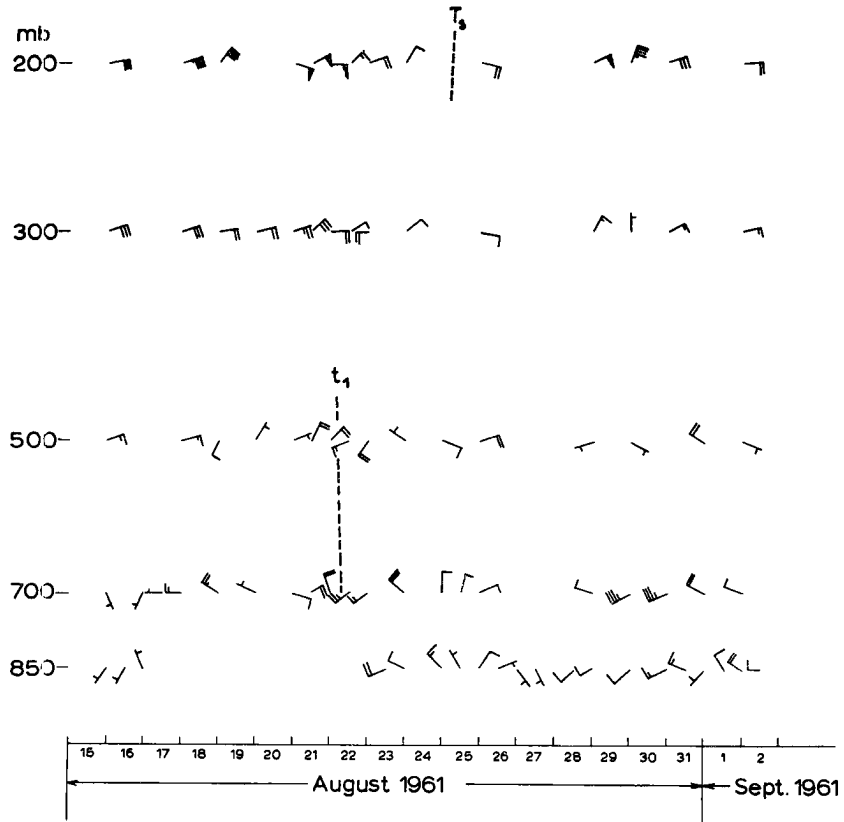
Fig. 11 Upper winds, Chiangmai.
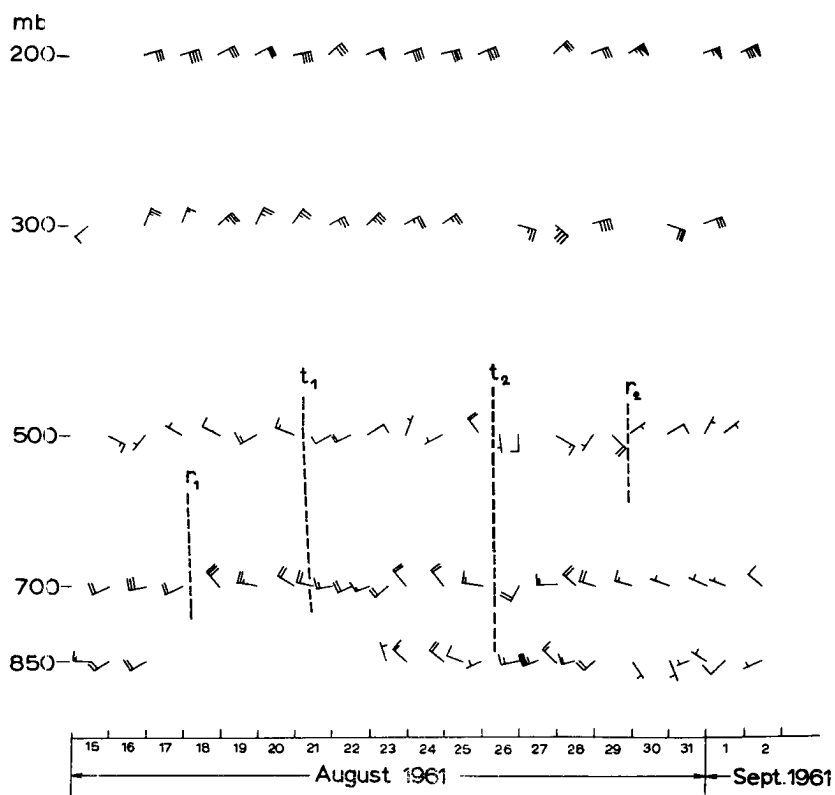
Fig. 12 Upper winds, Songkhla.
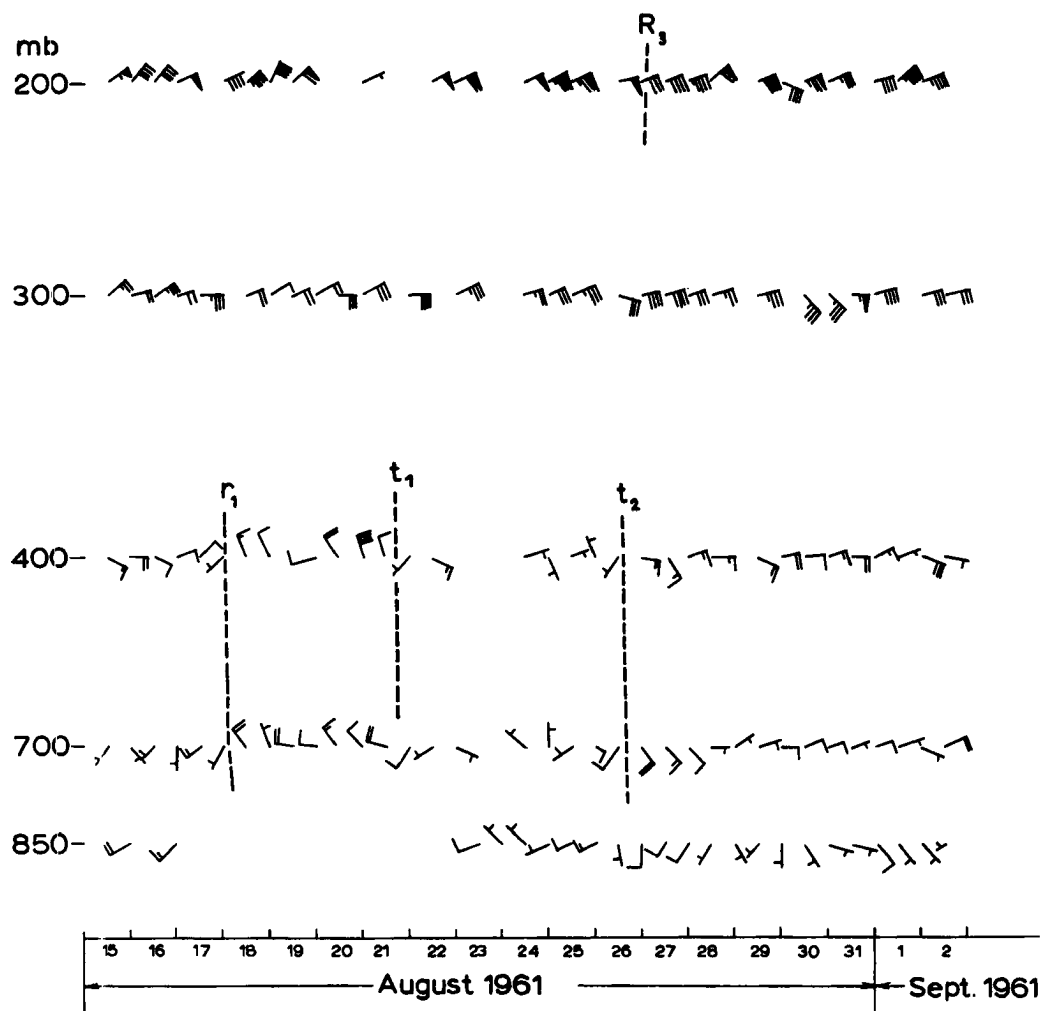
Fig. 13   Upper winds, Singapore.
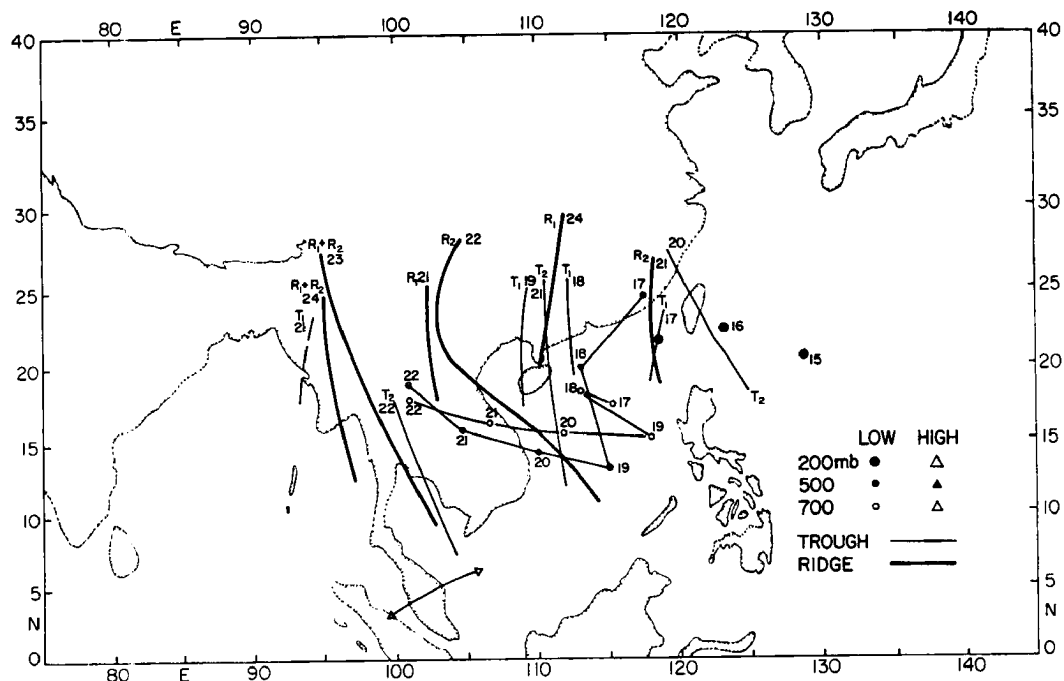
Fig. 14   Synoptic events, Aug. 15-24, 1961.
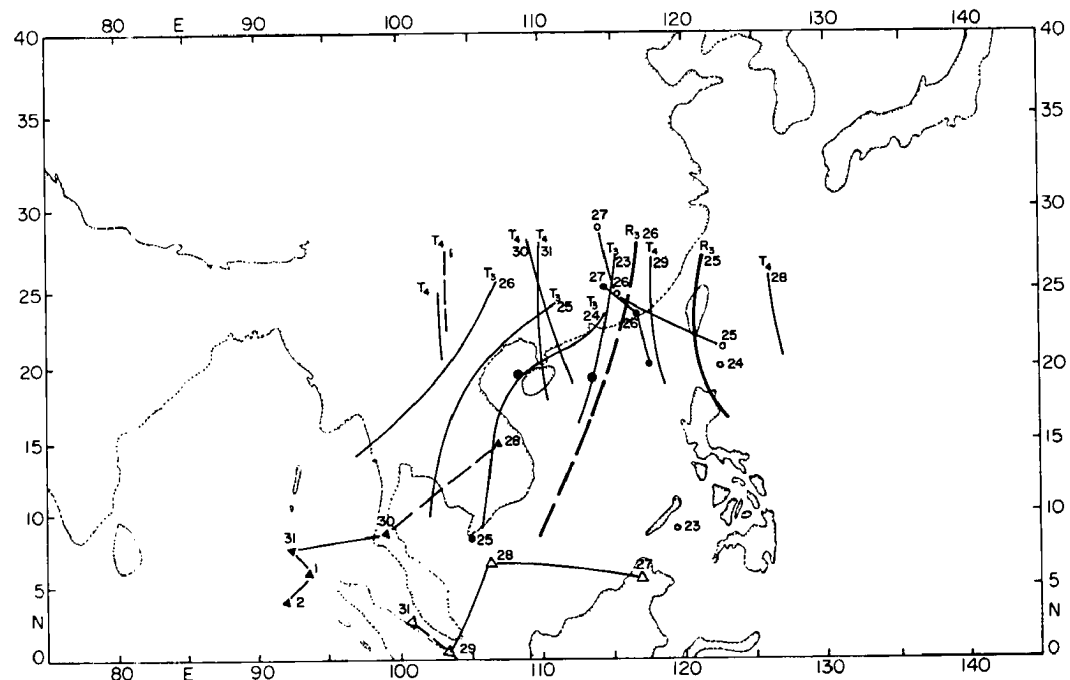
Fig. 15   Synoptic events, Aug. 23-Sept. 2, 1961.
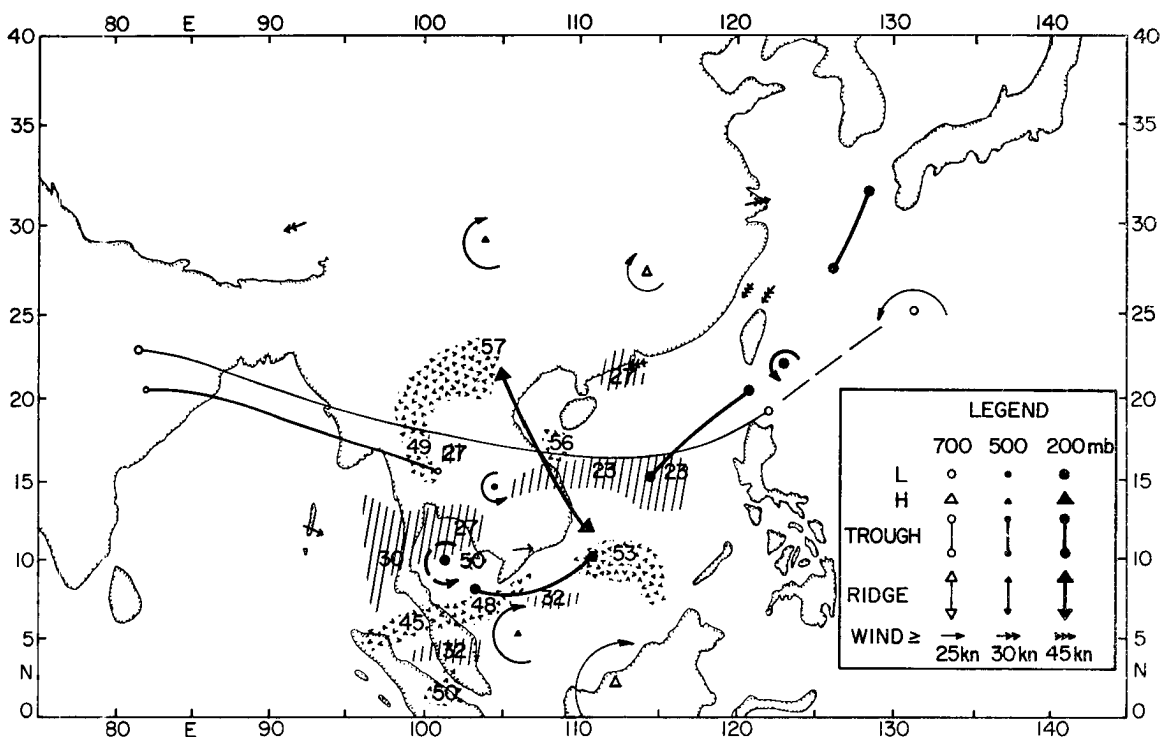
Fig. 16   Summary of synoptic and radiation conditions, Aug. 16, 1961.
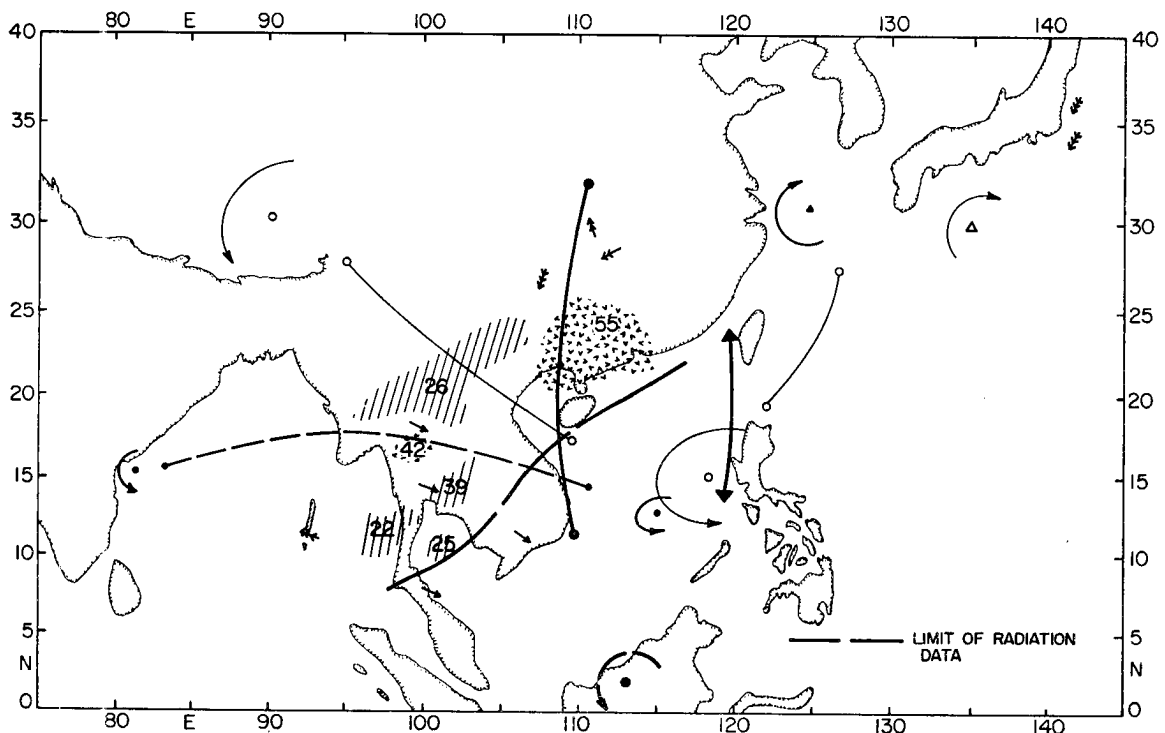
Fig. 17   19 August 1961.   Symbols as in Fig. 16.
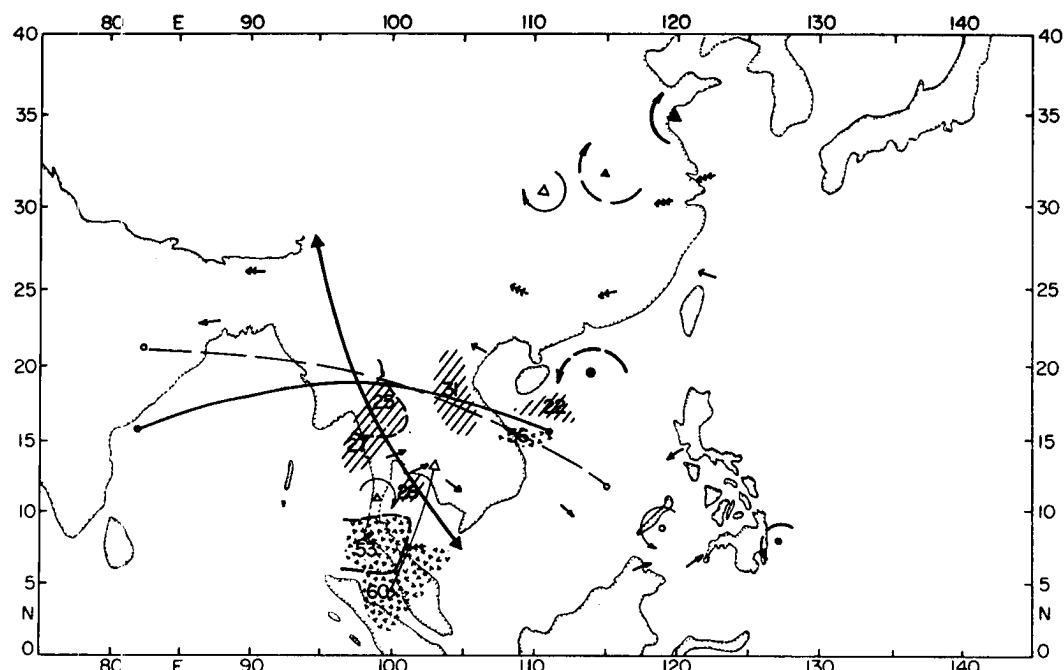
Fig. 18   23 August 1961; broken lines give radiation for midnight.
Other symbols as in Fig. 16.   Low and high radiation
areas given by shading.
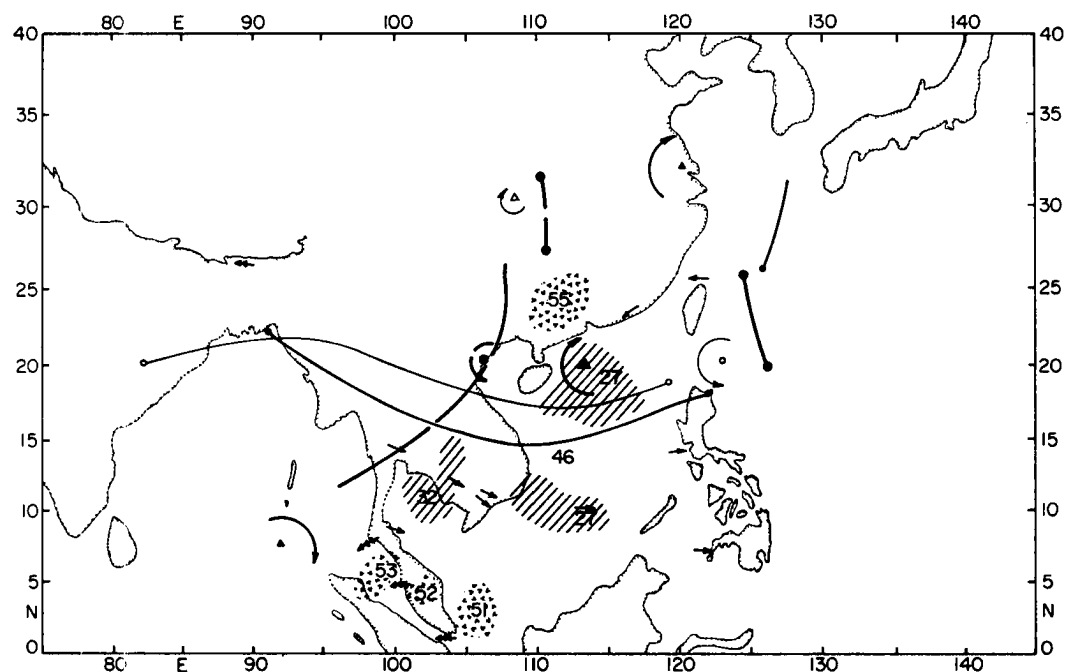
Fig. 19   24 August.   Symbols as in Fig. 16.
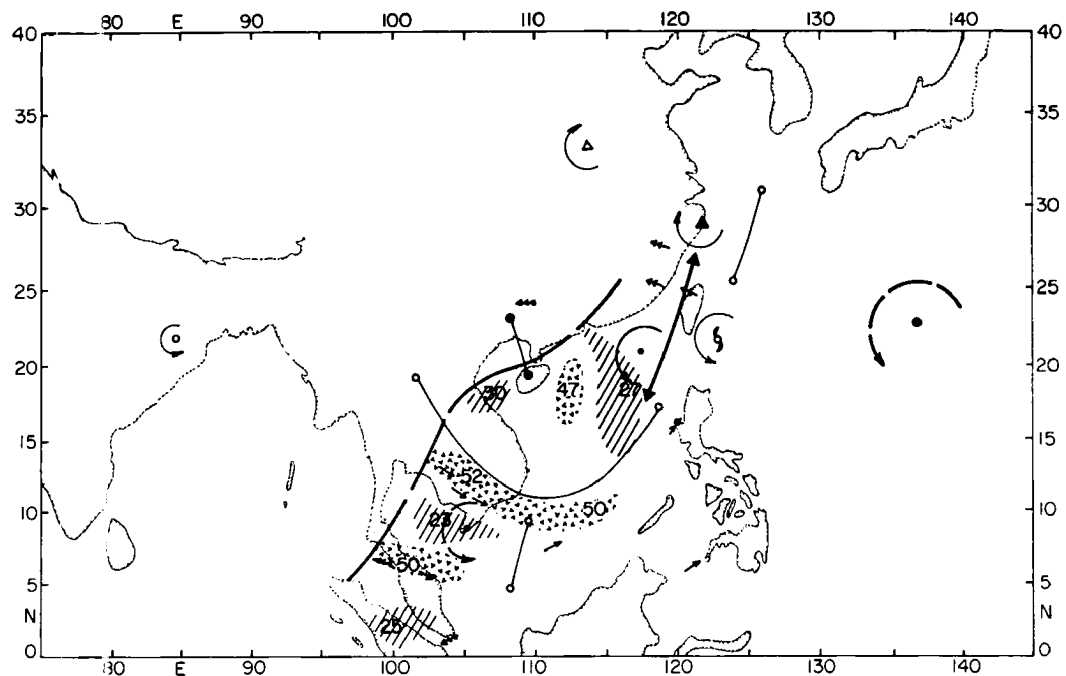
Fig. 20   25 August.   Symbols as in Fig. 16.
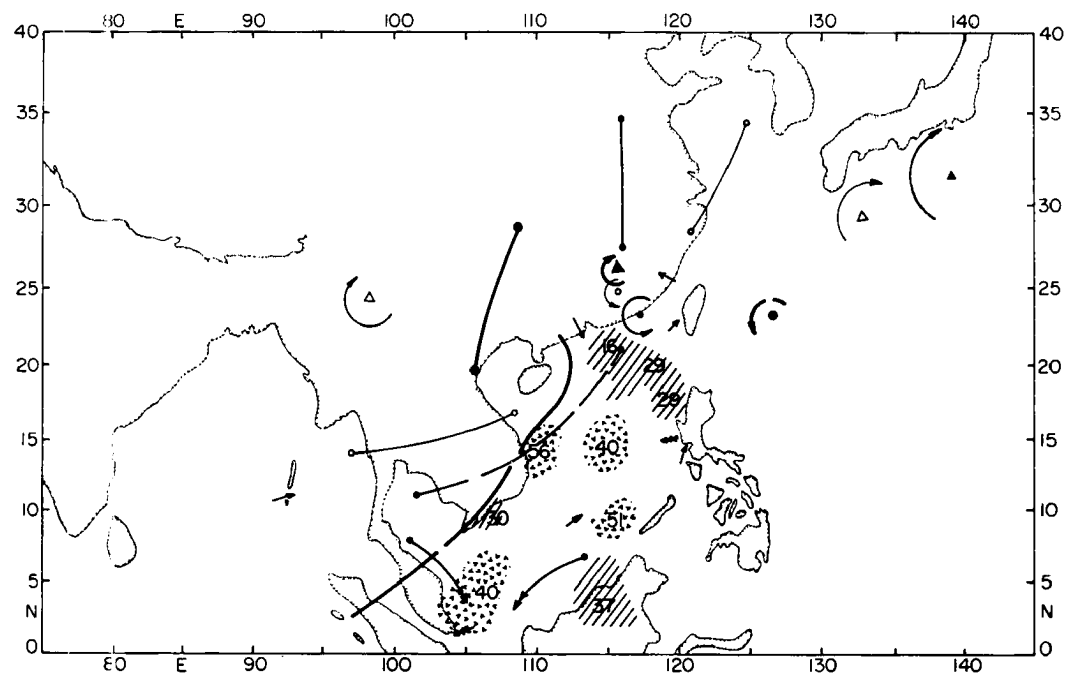
Fig. 21   26 August.   Symbols as in Fig. 16.
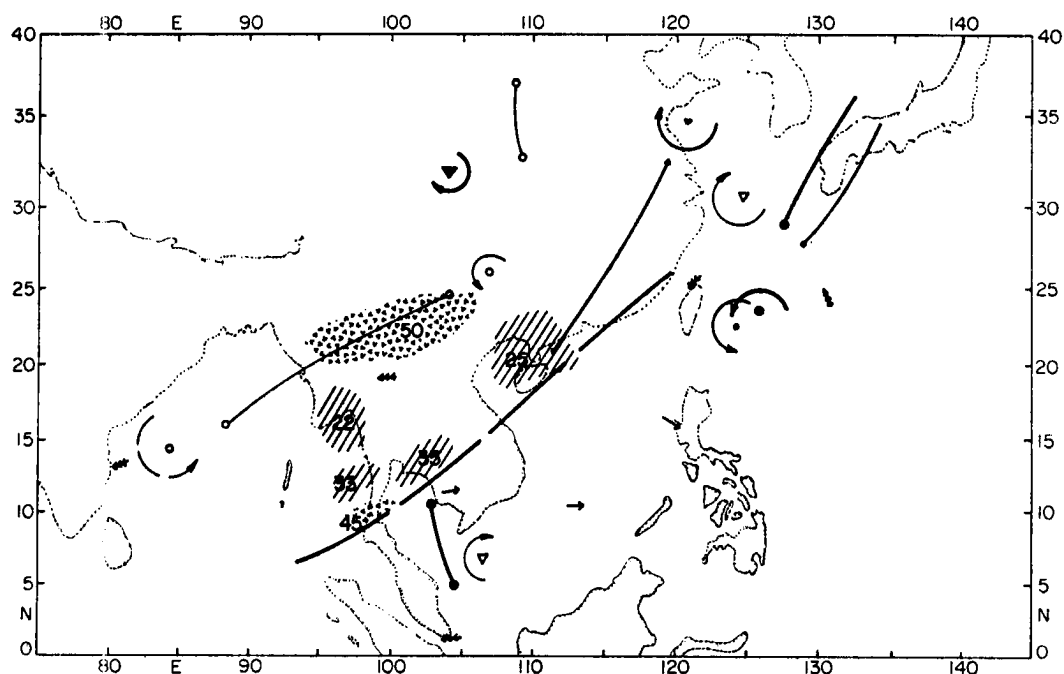
Fig. 22 28 August. Symbols as in Fig. 16.
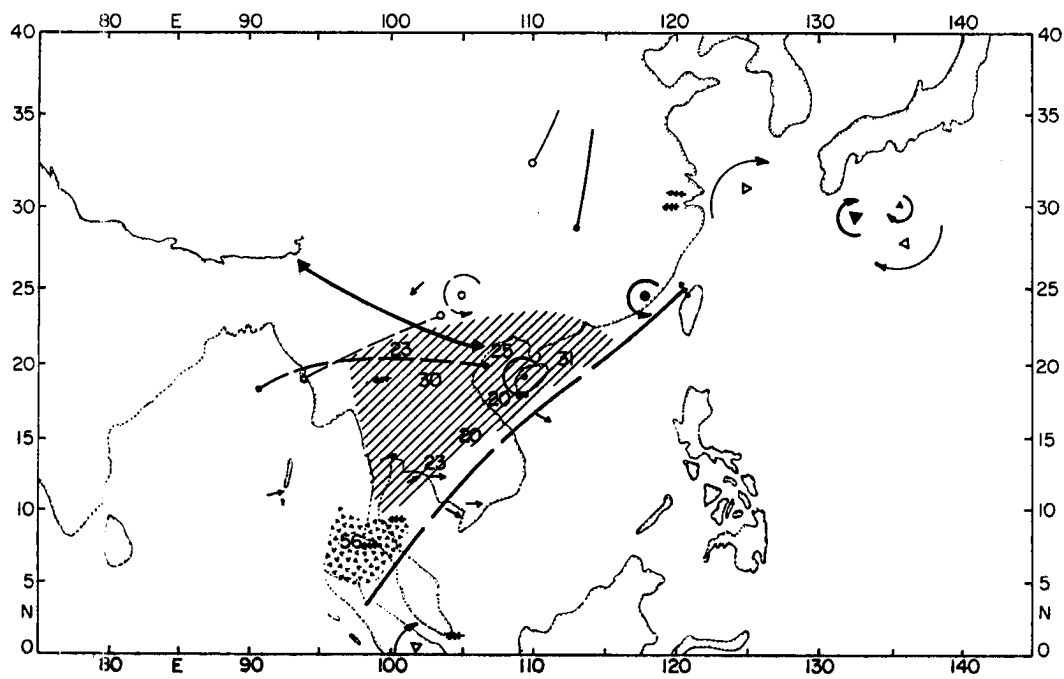
Fig. 23 29 August. Symbols as in Fig. 16.
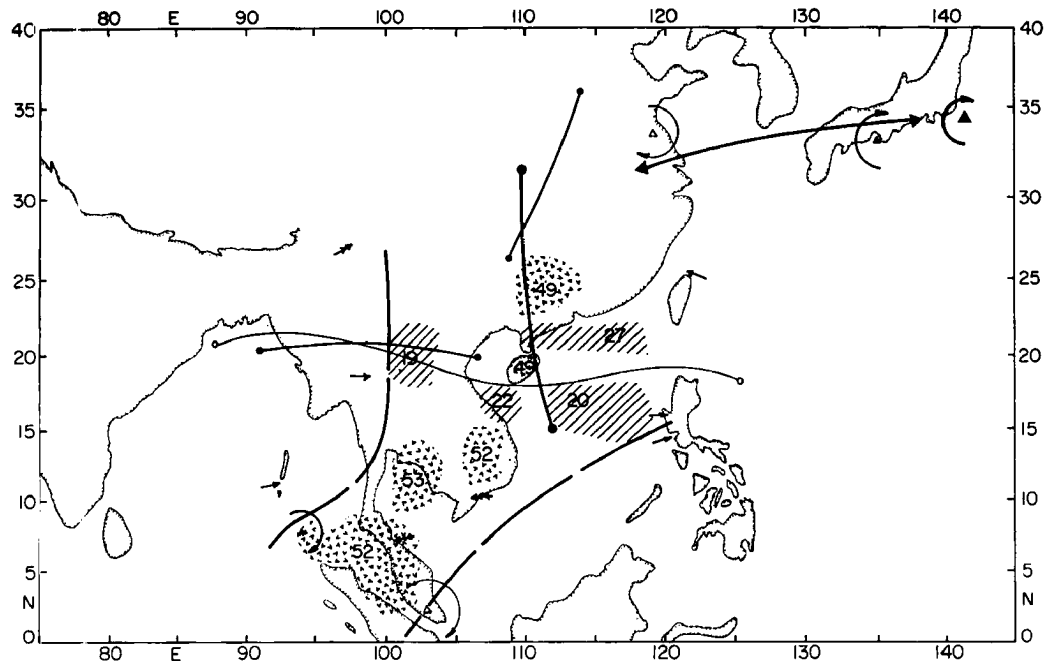
Fig. 24   31 August.   Symbols as in Fig. 16.
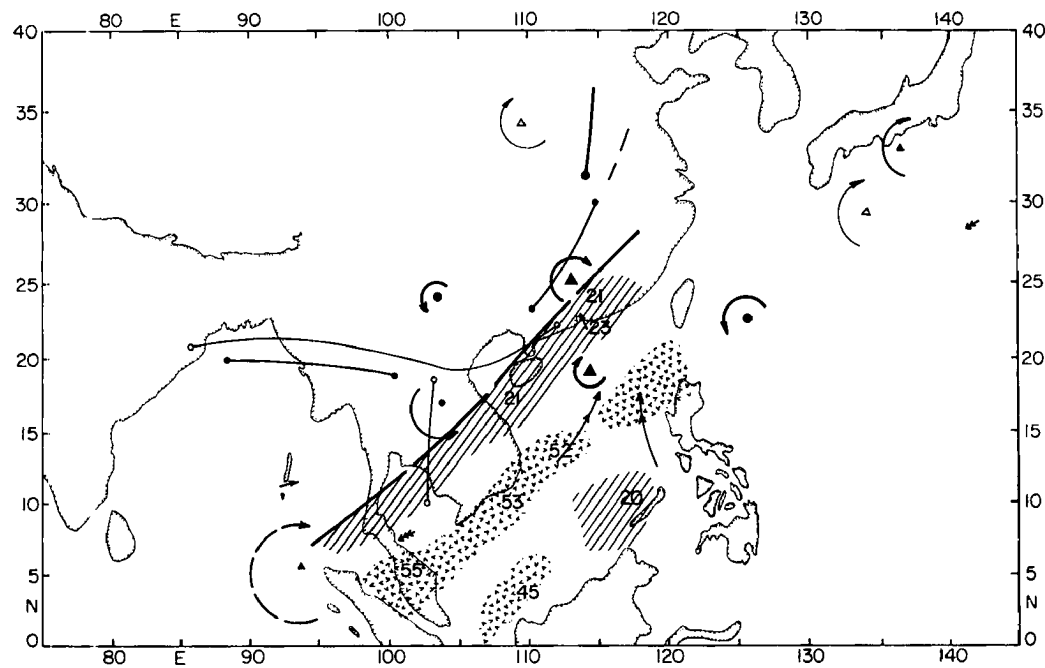
Fig. 25   1 September.   Symbols as in Fig. 16.
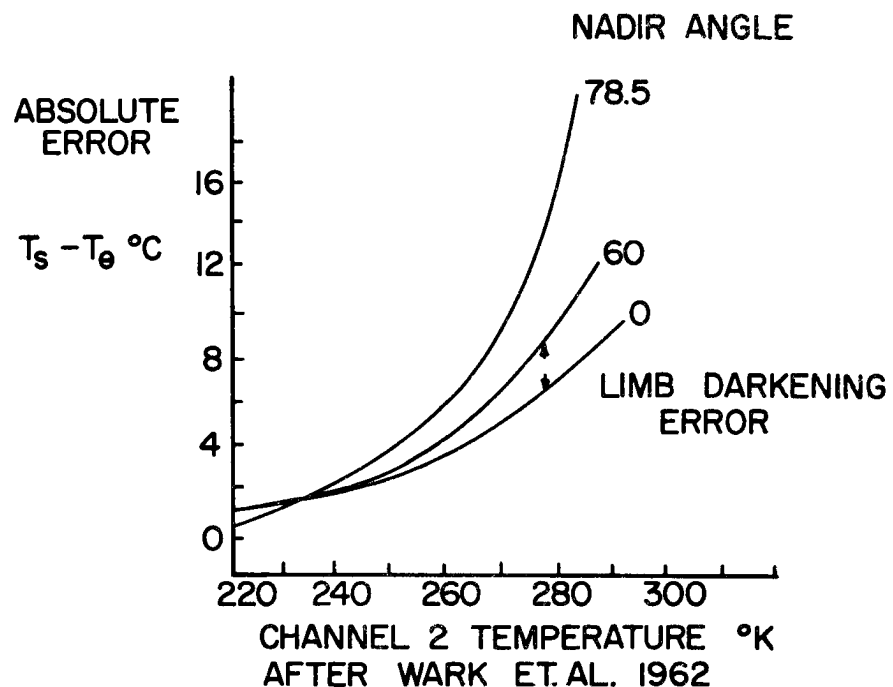
Fig. 26   Limb darkening of channel 2 radiation.
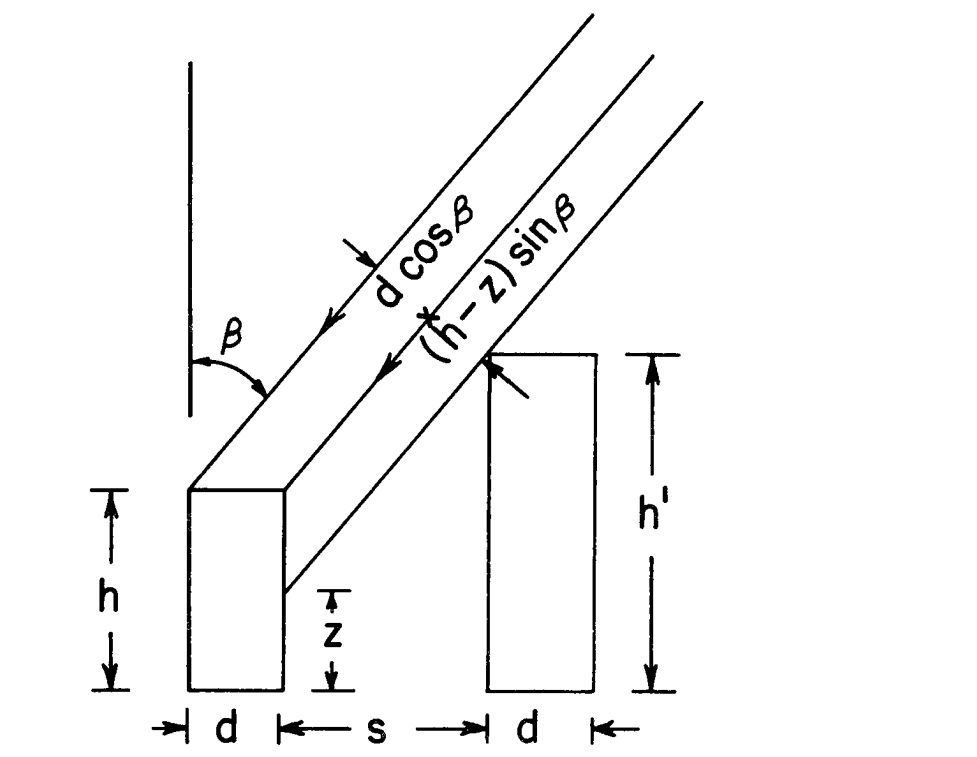
Fig. 27   Cloud field geometry.
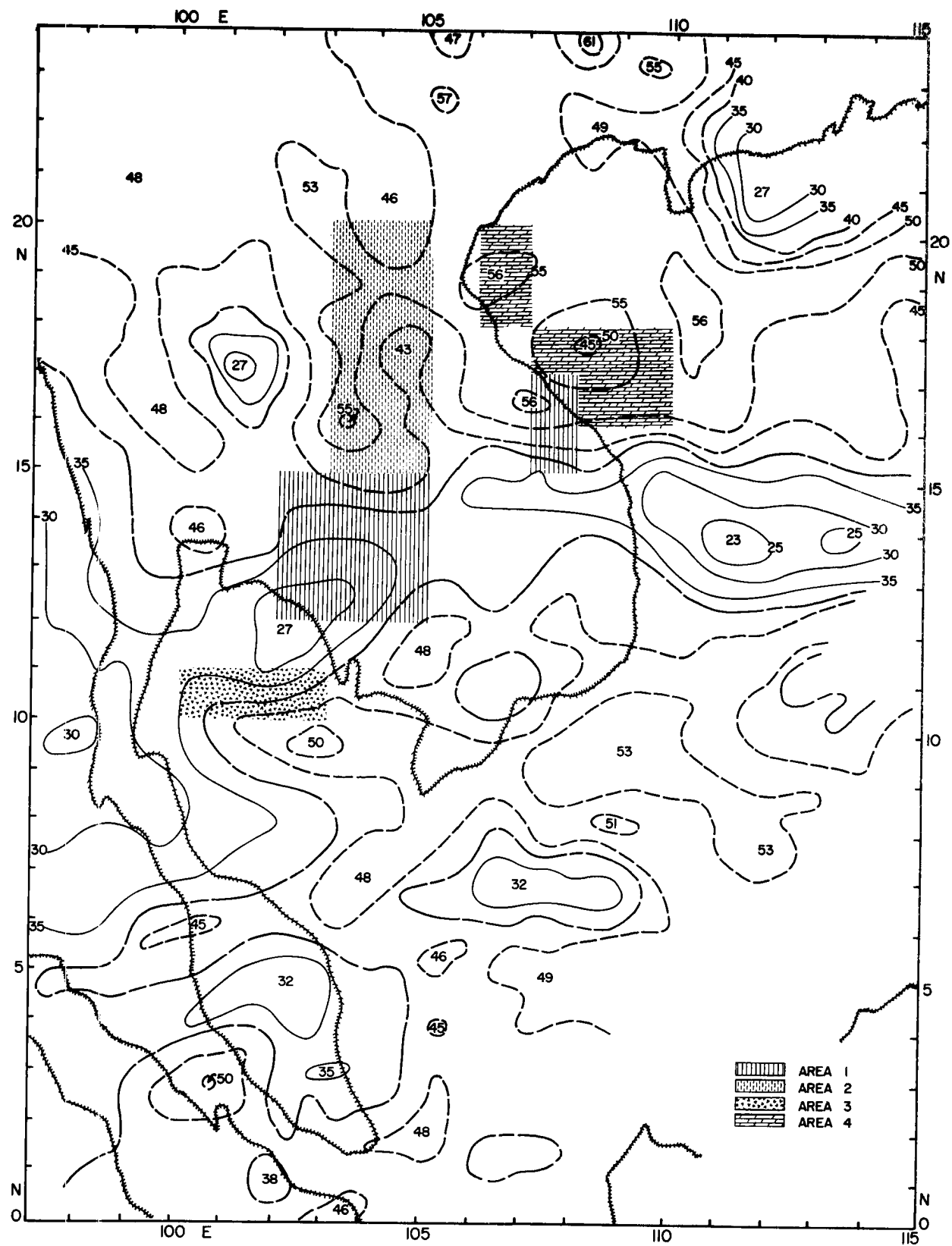
Fig. 29   Radiation surface and areas used for texture analysis.
Numbers give radiation intensities in 10^{-2} ly min.$^{-1}$
Tiros III Orbit 501 August 16, 1961, 15 GMT.
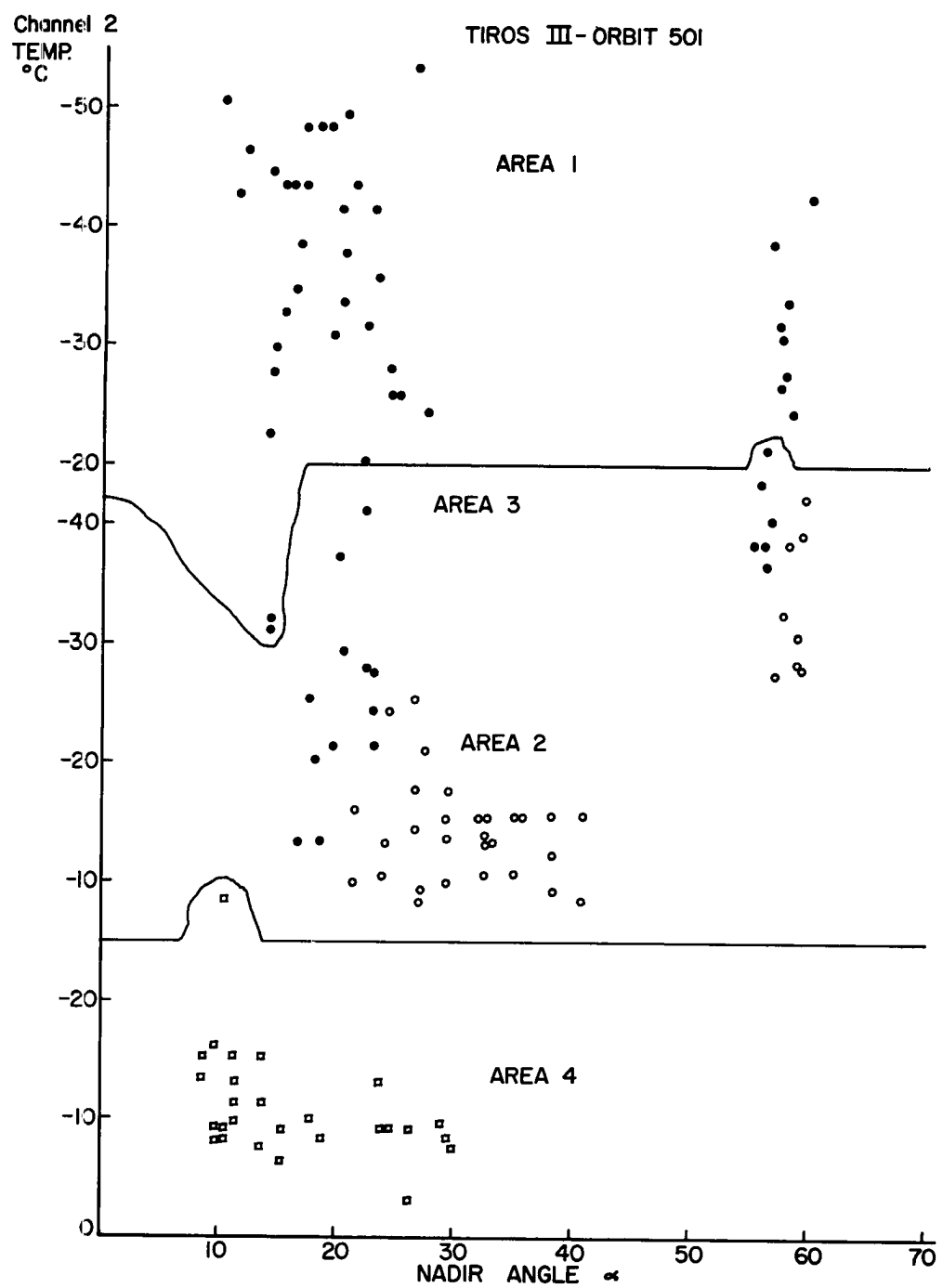
Fig. 30   Observed radiation surface textures.   Orbit 501
Tiros III.